Substrate and stereochemical control of peptidoglycan crosslinking by transpeptidation by *Escherichia coli* PBP1B

Anita C. Catherwood*[$], Adrian J. Lloyd*[+$], Julie A. Tod*, Smita Chauhan*, Susan E. Slade, Grzegorz Walkowiak*, Nicola F. Galley*, Avinash S. Punekar*, Katie Smart*, Dean Rea*, Neil D. Evans*, Michael J. Chappell*, David I. Roper* and Christopher G. Dowson*[+]

*School of Life Sciences, University of Warwick, Gibbet Hill Road, Coventry, CV4 7AL, UNITED KINGDOM.

+ corresponding Authors: AJL: Adrian.Lloyd@warwick.ac.uk; C.G.D: C.G.Dowson@warwick.ac.uk

[$]Both authors contributed equally to the manuscript

Supplementary Data

Contents

S.1: Supplementary Materials and Methods

S.1.1. Materials

Undecaprenyl phosphate was obtained from Larodan AB (Sweden), (((3R,5R,6R)-3-acetamido-4,5-dihydroxy-6-(hydroxymethyl)tetrahydro-2H-pyran-2-yl)methyl)phosphonic ((5-(2,4-dioxo-3,4-dihydropyrimidin-1(2H)-yl)-3,4-dihydroxytetrahydrofuran-2-yl)methyl phosphoric) anhydride (UDP:CH_2:GlcNAc) was synthesised by GVKBio (India). *D*-alanyl-*L*-alanine was synthesised by Activotec Ltd., UK. The pET 28a(+) expression construct for *Rhodotorula gracilis D*-amino acid oxidase was synthesised by Genescript[S1] and was a generous gift from Profesor N. Dale (School of Life Sciences, University of Warwick). *Corynebacterium glutamicum meso*-diaminopimelic acid (DAP) dehydrogenase was a generous gift from D.I.Roper (University of Warwick). *E. coli* MurA was expressed as described[S2]. Tomato etch virus (TEV) protease was a generous gift from D. Bellini (School of Life Sciences, Warwick University). An expression plasmid construct for *E. coli* MurG with a C-terminal hexahistidine tag (pDMC3) was a generous gift from J. van Heijenoort (Biochimie Structurale et Cellulaire, Université Paris-Sud, France). MurG was over-expressed from it and subsequently purified as described[S3]. The coding sequence for *Staphylococcus aureus* Mu50 monofunctional transglycosylase (residues 28-269) was cloned into pET15b[S4] and overexpressed as described[S5]. *Pseudomonas aeruginosa* MurB, MurC, MurD, MurE, MurF and *Streptococcus pneumoniae* MurE and MurF were purified as described[S6,S7]. *D*-isoglutamine was from Bayer. Biotinyl-N-hydroxysuccinamide ester and LCMS grade water were from Thermo Pierce. Isocitrate dehydrogenase (Porcine) was purchased from Sigma and was purified and quantitated as described[S7]. All immobilised metal affinity and ion exchange chromatography media were purchased from GE. All protease inhibitors, DNAse, hen egg white lysozyme, bovine thrombin, Triton X-100 (low peroxide grade), ethylene glycol-bis(β-aminoethyl ether)-N,N,N′,N′-tetraacetic acid (EGTA), chloroamphenicol, flavin adenine dinucleotide (FAD), lactitol, β-mercaptoethanol, pyridoxal phosphate, *L*-lysine and its

derivatives, all other *D* and *L* amino acids, dansyl chloride, *D*-alanyl-*D*-alanine, *D*,*L* isocitrate, horse radish peroxidase, porcine kidney *D*-amino acid oxidase, lactate dehydrogenase, rabbit muscle pyruvate kinase, phospho*enol* pyruvate, *Streptomyces globisporus* mutanolysin and hexa ethylene glycol dodecyl ether (E_6C_{12}) were purchased from Sigma. A racemic mixture of DAP was purchased from Sigma and individual *L*,*L*- and *meso*-stereoisomers of DAP were resolved and purified according to[S8]. Kanamycin, ampicillin, isopropyl β-*D*-1-thiogalactopyranoside (IPTG), 3-[(3-cholamidopropyl) dimethyl ammonio]-1-propane sulphonate (CHAPS), ampicillin, NADH, $NADP^+$, 2,2'-(propane-1,3-diyldiimino)bis [2-(hydroxymethyl)propane-1,3-diol] (*bis* Tris propane), 2-amino-2-(hydroxymethyl)propane-1,3-diol (Tris), and N-(2-hydroxyethyl) piperazine N'-(2-ethanesulfonic acid) (HEPES) were purchased from Melford. LCMS grade acetonitrile and methanol was from Honeywell Speciality Chemicals. LCMS grade formic acid was from Fisher. Mass spectrometry requisites (Sodium iodide calibrant, leucyl encephalin, sample manager vials and nanoflow probe tips) were from Waters Ltd. 1 ml Bond Elut CN-E reverse phase columns were from Agilent. Amplex Red (10-acetyl-3,7-dihydroxy phenoxazine) was from Invitrogen. Moenomycin was from Insight Biotechnology Ltd.

S.1.2. Methods

S.1.2.1. Protein analytical techniques

Sodium dodecyl sulphate-polyacrylamide gel electrophoresis and protein assays were performed according to[S9] and references therein.

S.1.2.2. Protein Purification

S.1.2.2.1. Purification of LpoB. The open reading frame corresponding to residues 22 to 213 of *E.coli* DH5α LpoB was cloned following methodology in[S9] between the Nco1/Xho1 sites of pPRoEX-Ha to yield pPROEX-EcLpoB. The integrity and authenticity of the LpoB over-expression construct was established by sequencing. *E. coli* LpoB was then expressed

from this plasmid in an *E.coli* BL21(DE3) strain as an N-terminal hexahistidine fusion protein with a TEV protease site between the hexahistidine sequence and the N-terminus of LpoB. Fresh transformants were grown overnight at 37°C in 100ml Luria Broth (LB) (10:5:5) and 0.1mg.ml^{-1} ampicillin. 1litre of fresh LB medium containing 0.2% (w/v) glucose and 0.1mg.ml^{-1} ampicillin was inoculated with a 1% (v/v) inoculum of overnight culture and grown at 37°C to an absorbance at 600 nm of 0.6. LpoB expression was induced by the addition of IPTG to 1mM and the culture were further incubated for 4 hours.

Cells were harvested by centrifugation at 10,000 x g, for 15 minutes at 4°C and resuspended in 20mM HEPES, pH7.4, 1M NaCl, 10% (v/v) glycerol, 200µM phenylmethyl sulfonylfluoride (PMSF), 1µM leupeptin and 1µM pepstatin (LpoB extraction buffer). A small amount of DNAse and 2.5 mg.ml^{-1} lysozyme were added and the suspension was gently agitated at 4°C for 30 minutes after which time, the cells were disrupted by sonication on ice in 10 cycles of 20 second bursts at 70% full power interspersed by 1 minute cooling on ice using a Bandelin Electronic sonicator. The insoluble material was removed by centrifugation at 50,000 x g for 45 minutes at 4°C and the supernatant was recycled at 4°C for 2 hours through a 5ml nickel-charged HisTrap FF column (GE Healthcare) that had been pre-equilibrated in LpoB extraction buffer. Bound proteins were eluted at 4°C at 1ml.min^{-1} with a 30 minute gradient of LpoB extraction buffer into the same buffer + 500mM imidazole. 2.5 ml fractions were collected and analysed by SDS-PAGE.

Selected fractions were exchanged into 20mM HEPES, pH 7.5, 0.5M NaCl, 10% (v/v) glycerol, 1 µM pepstatin, 200 µM PMSF (LpoB cleavage buffer) by centrifugal ultra-filtration using an Amicon Ultra-15 (3kD MWCO) membrane at 4°C. The His-tag was removed by incubation with 1 mg TEV protease/10mg fusion protein for 16 hours at 4°C. The cleaved protein was applied at 1ml.min^{-1} to a 5ml HisTrap FF column that was pre-equilibrated in LpoB cleavage buffer. Cleaved LpoB eluted in the flow through. LpoB-containing fractions were analysed by SDS PAGE and selected fractions were concentrated to 5 mg.ml^{-1} protein and stored in 0.5 ml aliquots at -80°C.

S.1.2.2.2. Purification of *E. coli* PBP1B. *E. coli* C43(DE3) was transformed with pDML924, a pET28a(+) derivative, with an open reading frame corresponding to the M46-N844 sequence of *E. coli* PBP1B, (PBP1Bγ isoform) which missed the cytoplasmic N-terminus (1-46) of the protein[S10]. The final coding sequence incorporated an N-terminal hexahistidine tag, followed by a thrombin cleavage site, followed by the PBP open reading frame. Positive transformants were cultured overnight at 37°C in Luria broth supplemented with 30 $\mu g.ml^{-1}$ kanamycin. The following day, one litre cultures of luria broth containing 30 $\mu g.ml^{-1}$ kanamycin and 2% (w/v) glucose were each inoculated with 10 ml of overnight culture and shaken at 200 rpm at 37°C until the absorbance at 600 nm reached 0.6-0.7. At this point, cultures were supplemented with 1 mM IPTG and incubated overnight at 25°C.

Adapting the methodology of[S11] *E. coli* cells were collected by centrifugation at 10,000 x g for 20 minutes at 4°C and resuspended at a ratio of 1 g cell pellet /5 ml of 25 mM Tris, 10 mM $MgCl_2$, 1 M NaCl, 1 mM EGTA pH 7.5, 1 μM pepstatin, 1 μM leupeptin, 2.5 $mg.ml^{-1}$ lysozyme and 5 $\mu g.ml^{-1}$ DNAse 1. Antifoam (2.5 $\mu l.ml^{-1}$) was added to the suspension which was disrupted in four passes through a cell disrupter at 30 kpsi. The suspension was centrifuged at 20,000 x g for 45 minutes at 4°C, and the supernatant was recentrifuged at 100,000 x g for 60 minutes at 4°C to collect *E. coli* membranes which were then resuspended in 25 mM Tris, pH 7.5, 10 mM $MgCl_2$, 1 M NaCl, 20% (v/v) glycerol and 8 mM CHAPS with gentle shaking for two hours.

This suspension was then centrifuged at 130,000 x g for 90 minutes at 4°C, and the supernatant was supplemented by 1 ml of cobalt-charged GE Healthcare Chelating Sepharose Fast Flow resin equilibrated in 25 mM Tris, pH 7.5, 10 mM $MgCl_2$, 1 M NaCl, 20% (v/v) glycerol and 1.3 mM CHAPS per litre of original culture. The suspension was gently agitated for one hour at 4°C, poured into a column, and eluted with 5 ml volumes of 25 mM Tris, pH 7.5, 10 mM $MgCl_2$, 1 M NaCl, 20% (v/v) glycerol and 1.3 mM CHAPS containing

sequentially 0, 15 and 50 mM imidazole, the concentration of which was then increased in 50 mM steps until a final wash containing 500 mM imidazole.

Fractions containing *E. coli* PBP1B were identified by SDS-PAGE and dialysed at 4°C against four changes of 1 litre of 25 mM Tris, pH 7.5, 10 mM $MgCl_2$, 1 M NaCl, 0.5 mM EGTA, 20% (v/v) glycerol and 0.27 mM CHAPS, pH 7.5. The protein was then supplemented with 36 units (Manufacturer's definition) of bovine thrombin and dialysis was continued with a further three changes of 1 litre of 25 mM Tris, pH 7.5, 10 mM $MgCl_2$, 1 M NaCl, 0.5 mM EGTA, 20% (v/v) glycerol and 0.27 mM CHAPS, pH 7.5 after one hour, overnight and finally for one hour. The protein was then dialysed at 4°C sequentially into10 mM sodium acetate pH 7.0, 1M NaCl, 10 mM $MgCl_2$, 10% (v/v) glycerol, 0.27 mM CHAPS and 0.02% (w/v) NaN_3 (two changes of 1 litre, 45 minutes each), 10 mM sodium acetate pH 6.0, 300 mM NaCl, 10 mM $MgCl_2$, 10% (v/v) glycerol, 0.27 mM CHAPS and 0.02% (w/v) NaN_3 (overnight) and finally, cation exchange buffer A + 0.1 M NaCl: 10 mM sodium acetate pH 5.0, 100 mM NaCl, 10 mM $MgCl_2$, 10% (v/v) glycerol, 0.27 mM CHAPS and 0.02% (w/v) NaN_3 (three changes of 1 litre every 30 minutes).

At this point, the protein was loaded at 2 $ml.min^{-1}$ at 4°C onto a HiTrap SP HP 5ml column equilibrated in cation exchange buffer A, and the column was washed in this buffer after which a gradient over 13 column volumes was applied into cation exchange buffer A + 2 M NaCl. Fractions containing the PBP were identified by SDS-PAGE and were dialysed at 4°C against three hourly changes of 1 litre of cation exchange buffer + 0.5 M NaCl. The protein was concentrated by centrifugal ultrafiltration to between 0.7 and 1 $mg.ml^{-1}$ protein in a 50,000 Da molecular weight cut-off Vivaspin centrifugal concentrator and snap frozen in 10 μl aliquots in liquid nitrogen for storage at -80°C.

S.1.2.2.3. Purification of *R. gracilis D* amino acid oxidase. The codon optimised cDNA coding sequence of D-amino acid oxidase inserted into pET 28a[S1] was transformed into *E. coli* BL21(DE3). Positive transformants were selected and cultured overnight at 37°C in Luria broth supplemented with 50 $\mu g.ml^{-1}$ kanamycin. The following day, four one-litre cultures of

luria broth containing 50 μg.ml^{-1} kanamycin were inoculated with 8 ml each of overnight culture and shaken at 180 rpm at 37°C until the absorbance at 600 nm reached 0.4. The temperature was reduced to 20°C and once the absorbance had reached 0.5, cultures were supplemented with 1 mM IPTG and a further 50 μg.ml^{-1} kanamycin and incubated for 4 hours at 20°C.

E. coli cells were collected by centrifugation at 6,000 x g for 20 minutes and resuspended in 50 mM Tris, 2 μM pepstatin, 200 μM PMSF and 5% (v/v) glycerol, pH 8.0, 3 mM FAD, 2.5 mg.ml^{-1} lysozyme and 5 μg.ml^{-1} DNAse 1. The suspension was sonicated on ice for ten 15 second bursts at 70% power intersperced by 1 minute cooling and centrifuged at 50,000 x g for 45 minutes at 4°C. The supernatant was loaded onto a 5-ml nickel-charged His-Trap HP column pre-equilibrated in 50 mM Tris, 0.3 M NaCl, 0.25 mM FAD and 5% (v/v) glycerol, pH 8.0. The column was washed at 4°C in the same buffer and the D-amino oxidase was eluted on a linear gradient over 10 column volumes into 50 mM Tris, 0.3 M NaCl, 0.25 mM FAD, 5% (v/v) glycerol and 0.5 M imidazole pH 8.0. The presence and purity of the D-amino acid oxidase in the imidazole eluted fractions was confirmed by SDS-PAGE.

Fractions were combined, and subjected to cycles of concentration and dilution with 50 mM Tris, 0.3 M NaCl, 0.25 mM FAD and 5% (v/v) glycerol, pH 8.0 in a 10,000 Da molecular weight cut-off Vivaspin centrifugal concentrator at 4,000x g at 4°C until the estimated imidazole concentration was ~37.5 μM. The concentrated protein was diluted into 50 mM Tris, 50 mM lactitol, 5 mM EDTA, 10% (v/v) glycerol and 25 μM FAD, pH 8.0 and concentrated to a protein concentration of greater than 60 mg.ml^{-1}. The FAD concentration of the sample was estimated in 50 mM sodium phosphate pH 7.0 at 450 nm ($\varepsilon_{1cm,\ 450\ nm}$ = 11,300 M^{-1}.cm^{-1})[S12]. Any shortfall in FAD concentration relative to that of D-amino acid oxidase was made good by addition of FAD to 1.1 times the molar deficit of sample FAD relative to sample D-amino acid oxidase.

S.1.2.2.4. Purification of *E. coli* B DacB (PBP4). The periplasmic domain of *E. coli* DacB (residue 21 to 477) cloned into the Nde1 and BamH1 sites of pET21b[S13] was transformed into *E. coli* BL21 star (DE3) pLysS. Positive transformants were cultured overnight at 37°C

in Luria broth supplemented with 50 μg.ml^{-1} ampicillin and 35 μg.ml^{-1} chloroamphenicol. The following day, one-litre cultures of luria broth containing 50 μg.ml^{-1} ampicillin and 35 μg.ml^{-1} chloroamphenicol were each inoculated with 10 ml of an overnight culture and shaken at 180 rpm at 37°C until the absorbance at 600 nm reached 0.4. The temperature was reduced to 25°C, cultures were supplemented with 0.5 mM IPTG, and re-supplemented further with 50 μg.ml^{-1} ampicillin and 35 μg.ml^{-1} chloroamphenicol and incubated for a further 4 hours at 25°C.

E. coli cells were collected by centrifugation at 6,000 x g for 20 minutes at 4°C, resuspended for 30 minutes in 50 mM Tris, 0.1 M NaCl, pH 8.5 and 2.5 mg.ml^{-1} lysozyme, sonicated on ice for ten 15 second bursts at 70% power interspersed by 1 minute cooling and centrifuged at 10,000 x g for 30 minutes at 4°C, where the resulting supernatant was centrifuged at 50,000 x g for a further 30 minutes at 4°C. The 50,000 x g supernatant was loaded at 3 ml.min^{-1} onto a 5 ml HiTrapQ fast flow anion exchange column at ambient temperature that was pre-equilibrated in 50 mM Tris, 0.1 M NaCl and 250 μM PMSF pH 8.5. The column was washed at 4°C in the same buffer and DacB was eluted on a linear gradient over 10 column volumes into 50 mM Tris, 0.5 M NaCl and 200 μM PMSF pH 8.5. The presence and purity of the DacB was confirmed by SDS-PAGE. Fractions were concentrated by dialysis into a storage buffer of 50 mM Tris, 0.2 M NaCl, 200 μM PMSF and 50% (v/v) glycerol pH 8.5.

S.1.2.2.5. Purification of *E. coli* Alanine Racemase. An over-expression construct for the *E. coli* alanine racemase gene was obtained as a generous gift from Professor C.W. Fishwick and Dr. Anil Agarwal (University of Leeds Dept. of Chemistry)[S14] and transformed into *E. coli* BL21 (DE3). Positive transformants were cultured overnight at 37°C in Luria broth supplemented with 50 μg.ml^{-1} ampicillin. The following day, six one-litre cultures of luria broth containing 50 μg.ml^{-1} ampicillin were each inoculated with 8 ml of overnight culture and shaken at 180 rpm at 37°C until the absorbance at 600 nm reached 0.6. The temperature was

reduced to 25°C, cultures were then supplemented with 0.5 mM IPTG, and incubated for a further 16 hours at 25°C.

E. coli cells were collected by centrifugation at 6,000 x g for 20 minutes at 4°C, resuspended with shaking for 30 minutes in 3 ml of 50 mM HEPES, 1 mM $MgCl_2$, 2 mM β-mercaptoethanol, 1 μM pepstatin, 1 μM leupeptin, 200 μM PMSF, 20 μM pyridoxal phosphate and 2.5 $mg.ml^{-1}$ lysozyme per gram (wet weight) of cell paste, sonicated on ice for ten 15 second bursts at 70% power intersperced by 1 minute cooling, centrifuged at 10,000 x g for 15 minutes at 4°C, where the supernatant was centrifuged at 50,000 x g for a further 30 minutes at 4°C. The 50,000 x g supernatant was loaded at 1 $ml.min^{-1}$ onto a 5 ml nickel-charged HisTrap HP column at 4°C pre-equilibrated in 50 mM HEPES, 1 mM $MgCl_2$, 0.5 M NaCl, 5% (v/v) glycerol, 1 μM pepstatin, 1 μM leupeptin, 200 μM PMSF and 20 μM pyridoxal phosphate pH 7.5. The column was washed at 4°C in 50 ml of the same buffer and alanine racemase was eluted on a linear gradient over 10 column volumes into the same buffer + 0.5 M imidazole. The presence and purity of the alanine racemase was confirmed by SDS-PAGE. Fractions were concentrated by dialysis into alanine racemase storage buffer (50 mM HEPES, 1 mM $MgCl_2$, 50 mM NaCl, 50% (v/v) glycerol, 1 μM pepstatin, 1 μM leupeptin, 200 μM PMSF, 100 μM pyridoxal phosphate pH 7.5).

The pyridoxal phosphate concentration of the sample was estimated in 50 mM sodium phosphate pH 7.0 at 388 nm ($\varepsilon_{1cm,\ 388\ nm}$ = 4,900 $M^{-1}.cm^{-1}$)**[S12]**. From this, any shortfall in pyridoxal phosphate concentration relative to that of alanine racemase was restored by increasing the concentration of the cofactor by 1.2 times the molar deficit of sample pyridoxal phosphate relative to sample alanine racemase.

S.1.2.3. Mass spectrometric analysis

S.1.2.3.1. Mass spectrometric nano-spray time of flight analysis of donor and acceptor substrates. Synthesis of all substrates were confirmed by negative ion time of flight mass spectrometric analysis using a Waters Synapt G2Si quadrupole-time of flight instrument

operating in resolution mode, equipped with a nanospray source calibrated with an error of less than 1 ppm with sodium iodide over a 200-2500 m/z range. Samples, prepared by dilution in LCMS grade solvents to between 1 μM and 5 μM in 50% (v/v) acetonitrile (Muramyl and UDP-muramyl peptides) or 7:3 methanol : 25 mM ammonium acetate (lipids), were introduced into the instrument using Waters thin wall nanoflow capillaries and up to 20 minutes of continuum data were collected at a capillary voltage of 2.0 kV, cone voltage of 100 V and a source offset of 41 V. Source and desolvation temperatures were 80°C and 150°C respectively, desolvation and purge gas flow rates were both 400 litres.min^{-1}. Scan time was one second with an interscan time of 0.014 seconds. Scans were combined into centred mass spectra by Waters Mass Lynx software. Resolution (m/z/half-height spectral peak width) was measured as 1 in 20,100.

S.1.2.3.2. Mass spectrometric *E. coli* PBP1B activity assays

S.1.2.3.2.1. LCMS/LCMSMS analysis of Transpeptidation. Here, substitution of Triton X-100 with an alternative detergent was required because the former was incompatible for mass spectral analysis due to its heterogeneous polymer length and consequent masking of relevant mass spectrometric output. Therefore a defined ethylene glycol detergent, 0.0416% (w/v) hexaethylene glycol dodecyl ether (E_6C_{12}, CMC 0.0036% (w/v)[S15]) was selected instead to replace Triton X-100 to support PBP1B activity in assays destined to be analysed by LCMS.

In this case, assays to be subjected to mass spectral analysis were initially performed spectrophotometrically (main paper Methods), except that the lipid II donor was added to a final concentration of 20 μM from a 0.2 mM stock reconstituted in 0.026 % (w/v) E_6C_{12} and *E. coli* PBP1B was diluted into 25 mM Tris, 0.0519% (w/v) E_6C_{12}, 10% (v/v) glycerol, pH 7.5. In these experiments, assays were continuously monitored at 555 nm and were performed such that the lipid II donor was present at the beginning of the assay. After 2 minutes had elapsed, *E. coli* PBP1B was added and the absorbance was followed for a further 6 minutes, at which point, 20 μM lipid or MurNAc DAP peptide acceptor (if required) was then added. After

monitoring the reaction for a further 20 minutes, the 0.2 ml assay was treated with 20 μl 2.2 M *bis*-Tris pH 6.0 and 20 μl of a freshly prepared stock of 10 $mg.ml^{-1}$ mutanolysin (prepared in 10 mM HEPES, 2.5 mM $MgCl_2$, pH 7.6). The sample was incubated for two hours at 37°C, resupplemented with a further 20 μl of 10 $mg.ml^{-1}$ mutanolysin and incubated for an additional two hours. At this point, samples were boiled for 10 minutes and acidified with 24 μl of 20% (v/v) phosphoric acid. Samples were freeze dried, and resuspended in 0.1 % (v/v) formic acid for subsequent LCMS or LCMSMS analysis.

LCMS analysis was performed where 5 μl samples were delivered from glass vials from a Waters M-class sample manager through a Waters Acuity UPLC BEH 300 Å 1.7 μm C18 column (2.1 x 50 mm) that had been equilibrated in 99:1 water + 0.1% (v/v) formic acid (solvent A) : acetonitrile + 0.1% (v/v) formic acid (solvent B) at a flow rate of 50 $\mu l.min^{-1}$ through an electrospray source into a Waters Synapt G2Si quadrupole-time of flight instrument. The column was developed at the same flow rate at 20°C with a 1% (v/v) to 37% (v/v) gradient into solvent B over 30 minutes, followed by an increase in solvent B to 90% (v/v) over 1 minute. The column was washed for a further three minutes at 90% (v/v) solvent B, and returned to 1 % B (v/v) over the next minute and held at these conditions for a further 6 minutes. The first minute of elution was diverted to waste, whilst the remainder of the elution entered the mass spectrometer which was calibrated to less than 1 ppm with sodium iodide operating in positive ion in resolution mode. Total ion chromatographs were collected over 40 minutes at a capillary voltage of 2.5-3.0 kV, sampling cone voltage of 25 V, source offset of 80 V. Source and desolvation temperatures were 80°C and 150°C respectively, desolvation gas flow rate was 350 $litres.min^{-1}$. Scan time was 0.5 seconds over an m/z range of 200-2000 m/z with an interscan time of 0.014 seconds. Scans were converted to centred mass spectra by Waters Mass Lynx software. Resolution (m/z/half-height spectral peak width) was measured as 1 in 20,100. Calibration was maintained and automatically corrected every minute by switching the electrospray probe for 0.25 seconds between the eluant from the column and a 10 $\mu l.min^{-}$

[1] stream of leucyl encephalin (Lock Mass; $(m+H^+)/1$ = 556.277), delivered continuously at a capillary voltage of 3 kV.

LCMSMS analysis was performed on the basis of collision-induced fragmentation. Capillary, sampling cone, source offset voltages, source/desolvation temperatures and source gas flow rates were unchanged relative to their LCMS settings, and lock mass with leucyl encephalin was applied although the scan time for m/z 200-2500 was increased to 1 second. Calibration was with sodium iodide. Collision-induced fragmentation of species with the desired m/z (up to six) was performed in the trap cell of the mass spectrometer with an argon flow of 2 $ml.min^{-1}$ at a constant trap collision energy of 40 eV.

S.1.2.3.2.2. Negative ion Nanospray -Time of flight analysis of Transglycosylation. In this case, assays destined for mass spectral analysis of transglycosylation activity were initially performed spectrophotometrically using transpeptidation as reported by resorufin production at 555 nm as an indirect confirmation of transglycosylation. Fractionation of these assays and detection of undecaprenyl pyrophosphate was then used to assay transglycosylation.

Therefore, assays were performed in an identical manner to those designed to be subsequently analysed by mass spectrometry for transpeptidation products (**S.1.2.3.2.1.**) up until the point immediately prior to the addition of *bis*-Tris where 50 μM moenomycin was added in its place. At this juncture, adapting the methodology of Mesleh *et al*.[S16], assays were loaded onto 1 ml Bond Elut CN-E reverse phase columns that had been pre-equilibrated in 10 ml of 2:1 propan-2-ol:methanol and then 10 ml of water. Columns were then washed sequentially with 0.5 ml of water, and then 0.5 ml of 10, 20, 30, 40, 50, 60, 70, 80, 90% (v/v) 2:1 propan-2-ol:methanol in water and finally 100% (v/v) 2:1 propan-2-ol:methanol. Washes were then analysed for the presence of lipid II-Lys and undecaprenyl pyrophosphate by negative ion nano-spray time of flight mass spectrometry (expected (m-1)/1 = 925.62) as described in **S.1.2.3.1.**

S.1.2.4. *E. coli* PBP1B transpeptidase donor and acceptor substrate Preparation

S.1.2.4.1. Preparation of transpeptidation donor substrates. All lipid substrates were prepared via enzymatic synthesis of their UDP-MurNAc pentapeptide precursors: Lipid II-Lys and Lipid II-*meso*-DAP were prepared exactly as described[S7]. Lipid II-Lys with an amidation on the stem peptide glutamate α-carboxyl was prepared as described for lipid II-Lys, except that 22.9 mM *D*-glutamate was substituted by 105 mM *D*-*iso*-glutamine in the synthesis of the UDP-MurNAc pentapeptide precursor.

Lipid II with a third position stem peptide substitution of the lysyl moiety for *L*-arginyl (lipid II-Arg), 5 hydroxyl *L*-lysyl (lipid II-^{5}OH-Lys) and $^{\varepsilon}$N-methyl-lysyl (lipid II-Lys-CH_3) were prepared as described for lipid II-Lys[S7], where 15 mM *L*-lysine was substituted by 35 mM *L*-arginine, 5 hydroxyl *L*-lysine or $^{\varepsilon}$N-methyl-lysine in the synthesis of the UDP-MurNAc pentapeptide precursor.

Lipid II-Lys with the third position lysyl ε-amino dansylated (lipid II-$^{\varepsilon}$N-dansyl-Lys) was prepared by reaction of UDP-MurNAc *L*-alanyl-γ-*D*-glutamyl-*L*-lysyl-*D*-alanyl-*D*-alanine with dansyl chloride essentially as described[S17] which was then coupled to undecaprenyl phosphate and glucosaminylated[S7] to form lipid II-$^{\varepsilon}$N-dansyl-Lys.

To prepare Lipid II-Lys with the third position lysyl ε-amino biotinylated (lipid II-$^{\varepsilon}$N-biotinyl-Lys), UDP-MurNAc *L*-alanyl-γ-*D*-glutamyl-*L*-lysyl-*D*-alanyl-*D*-alanine was first freed of residual ammonium acetate. Therefore the nucleotide was loaded onto a 30 ml-column of Source 30Q anion exchange resin pre-equilibrated in 10 mM sodium bicarbonate pH 9.0[S18]. The nucleotide was eluted in 0.25 M sodium bicarbonate pH 9.0 and removal of contaminating ammonium acetate was confirmed by assay with Nessler's Reagent[S19]. The nucleotide was then added at a volume (molar) ratio of 2 (10) parts peptide to 1 (1) part biotinyl-N-hydroxy-succinamide ester in DMSO. The reaction was maintained at room temperature overnight and was quenched with a 10-fold molar excess of Tris, pH 9.0 over the biotin reagent. The sample was diluted four fold into 10 mM ammonium acetate pH 7.6, purified by anion exchange chromatography and converted to its lipid II-Lys derivative as described[S7].

Lipid II-Lys with a stem peptide where the C-terminal dipeptide was *D*-alanyl-*L*-alanine was synthesised as described[S7] for the canonical *D*-alanyl-*D*-alanine terminated lipid II-Lys where the synthesis of the UDP-MurNAc pentapeptide precursor was modified by substitution of *D*-alanyl-*D*-alanine with 15 mM *D*-alanyl-*L*-alanine (Activotec).

Lipid II-*L*,*L*-DAP was prepared as described for lipid II-*meso*-DAP where 35 mM *meso*-DAP was replaced by 5.6 mM *L,L*-DAP in the synthesis of the UDP-MurNAc pentapeptide precursor. Alternatively, lipid II-*L,L*-DAP was prepared in the presence of DAP dehydrogenase to eliminate insertion of any residual contaminating *meso*-DAP into the stem peptide. In this case, the synthesis of the UDP-MurNAc-*L*-alanyl-γ-*D*-glutamyl-*L,L*-DAP-*D*-alanyl-*D*-alanine precursor of Lipid II-*L*,*L*-DAP was performed in two stages. Firstly, 50 mM HEPES, 10 mM $MgCl_2$, 1 mM dithiothreitol, 50 mM KCl, 8.35 mM UDP-GlcNAc, 0.185 M phospho*enol*pyruvate, 7.83 μM *E. coli* MurA, 0.2 mM $NADP^+$, 26.5 mM *D*,*L*-isocitrate, 1.125 $U.ml^{-1}$ isocitrate dehydrogenase, 4.49 μM *P. aeruginosa* MurB, 6 mM ATP, 5.53 $U.ml^{-1}$ (manufacturer's unit definition) rabbit muscle pyruvate kinase, 35 mM *L*-alanine, 7.50 μM *P. aeruginosa* MurC, 35 mM *D*-glutamate, 13.5 μM *P. aeruginosa* MurD, 16.44 mM *L,L*-DAP, 35 mM *D*-alanyl-*D*-alanine and 1.0 $mg.ml^{-1}$ *C. glutamicum meso*-DAP dehydrogenase were incubated for two hours at 37°C. Then 25.7 μM *P. aeruginosa* MurE and 10.66 μM *P. aeruginosa* MurF were added and the incubation was continued overnight at 37°C. The following morning, the proteins were removed by centrifugal ultrafiltration through a Viva Spin centrifugal concentrator with a 10,000 molecular weight cut-off at 4°C. The filtrate was diluted four fold into 10 mM ammonium acetate pH 7.5 and loaded onto a 75 ml column of Source 30Q anion exchange resin equilibrated in the same buffer. The column was washed at 10 $ml.min^{-1}$ in 10 mM ammonium acetate pH 7.5 and UDP-MurNAc-*L*-alanyl-γ-*D*-glutamyl-*L,L*-DAP-*D*-alanyl-*D*-alanine was eluted in a 10 column volume gradient comprising 10 mM to 500 mM ammonium acetate, pH 7.5. The conversion of UDP-MurNAc-*L*-alanyl-γ-*D*-glutamyl-*L,L*-DAP-*D*-alanyl-*D*-alanine to Lipid II-*L*,*L*-DAP was then exactly as described for the synthesis of lipid II-Lys[S7].

Lipid II-*L*,*L*-$^{\varepsilon}$NAc-DAP and lipid II-*meso*-εNAc-DAP (Lipid II DAP acetylated on the ε–amino group of the *meso* or *L*,*L*-DAP inserted into the stem peptide of lipid II-DAP) were prepared from UDP-MurNAc-*L*-alanyl-γ-*D*-glutamyl-*L,L*-DAP-*D*-alanyl-*D*-alanine and UDP-MurNAc-*L*-alanyl-γ-*D*-glutamyl-*meso*-DAP-*D*-alanyl-*D*-alanine respectively. In both cases, the UDP MurNAc peptides were loaded onto a 30 ml-column of Source 30Q anion exchange resin pre-equilibrated in 10 mM sodium bicarbonate pH 9.0, eluted in 0.25 M sodium bicarbonate pH 9.0[S18] and confirmed free of residual ammonium acetate with Nessler's Reagent[S19]. Using absorbance at 260 nm to estimate the nucleotide concentration ($\varepsilon_{1cm,\ 260nm}$ = 10000 $M^{-1}.cm^{-1}$)[S12], a fifty-fold molar excess of acetic anhydride was then added to both UDP MurNAc pentapeptides which were stirred overnight at room temperature in the dark. The following morning, the reactions were diluted ten-fold into 10 mM ammonium acetate pH 7.5 and purified on a 75 ml column of Source 30Q anion exchange resin equilibrated in the same buffer. The column was washed at 10 $ml.min^{-1}$ in 10 mM ammonium acetate pH 7.5 and UDP-MurNAc-*L*-alanyl-γ-*D*-glutamyl-*L,L*-($^{\varepsilon}$N-acetyl)-DAP-*D*-alanyl-*D*-alanine or UDP-MurNAc-*L*-alanyl-γ-*D*-glutamyl-*meso*-($^{\varepsilon}$N-acetyl)-DAP-*D*-alanyl-*D*-alanine were eluted in a 10 column volume gradient comprising 10 mM to 500 mM ammonium acetate, pH 7.5. Confirmation of the synthesis of the acetylated UDP MurNAc pentapeptides was established by nanospray mass spectrometry (**S.1.2.3.1**). UDP-MurNAc-*L*-alanyl-γ-*D*-glutamyl-*L,L*-($^{\varepsilon}$N-acetyl)-DAP-*D*-alanyl-*D*-alanine and UDP-MurNAc-*L*-alanyl-γ-*D*-glutamyl-*meso*-($^{\varepsilon}$N-acetyl)-DAP-*D*-alanyl-*D*-alanine were then converted to their corresponding lipid II species (lipid II-*L*,*L*-$^{\varepsilon}$NAc-DAP and lipid II-*meso*-$^{\varepsilon}$NAc-DAP respectively) according to[S7].

The purity of all lipid products was established by TLC according to Breukink *et al*.[20], and their synthesis and that of their UDP-MurNAc precursors was confirmed by negative ion nano-spray time-of-flight mass spectrometry on a Waters Synapt G2Si Q-Tof mass spectrometer (Below).

S.1.2.4.2. Preparation of transpeptidation acceptor substrates. Lipid II *meso*-DAP tetrapeptide and Lipid II-*L,L*-DAP tetrapeptide was synthesised in three stages: UDP-MurNAc *meso*-DAP pentapeptide or its *L*,*L*-DAP derivative were synthesised and purified as described[S7] where for the *L*,*L*-DAP and *meso*-DAP containing nucleotides, 5.6 mM *L,L*-DAP and 35 mM *meso*-DAP was used respectively. Purified nucleotides were then cleaved to their tetrapeptide derivatives with DacB whereby in a final volume of 2 ml of 50 mM HEPES and 10 mM $MgCl_2$ adjusted to pH 7.6, 4.19 mM UDP-MurNAc-*L*-alanyl-γ-*D*-glutamyl-*L,L*-DAP-*D*-alanyl-*D*-alanine or UDP-MurNAc-*L*-alanyl-γ-*D*-glutamyl-*meso*-DAP-*D*-alanyl-*D*-alanine were incubated with 0.97 $mg.ml^{-1}$ of DacB overnight at 37°C. The following morning, DacB was removed by centrifugal ultrafiltration through a Viva Spin centrifugal concentrator with a 10,000 molecular weight cut-off at 4°C. The filtrate was diluted four fold into 10 mM ammonium acetate pH 7.5 and loaded onto a 75 ml column of Source 30Q anion exchange resin equilibrated in the same buffer. The column was washed at 10 $ml.min^{-1}$ in 10 mM ammonium acetate pH 7.5 and UDP-MurNAc-*L*-alanyl-γ-*D*-glutamyl-*L,L*-DAP-*D*-alanine or UDP-MurNAc-*L*-alanyl-γ-*D*-glutamyl-*meso*-DAP-*D*-alanine was eluted in a 10 column volume gradient of 10 mM to 500 mM ammonium acetate, pH 7.5 and identified by negative ion nano-spray time-of-flight mass spectrometry. The conversion of either stereoisomer of UDP-MurNAc-*L*-alanyl-γ-*D*-glutamyl-DAP-*D*-alanine to Lipid II-*L*,*L*-DAP tetrapeptide or Lipid II-*meso*-DAP tetrapeptide was then as described for synthesis of lipid II-Lys[S7].

Muramyl stem peptides MurNAc-*L*-alanyl-γ-*D*-glutamate, MurNAc-*L*-alanyl-γ-*D*-glutamyl-*meso*-DAP, MurNAc-*L*-alanyl-γ-*D*-glutamyl-*meso*-DAP-*D*-alanine and MurNAc-*L*-alanyl-γ-*D*-glutamyl-*meso*-DAP-*D*-alanyl-*D*-alanine were synthesised as their UDP-precursor derivatives[S7,S21], resuspended at a pH of 1.5 in 0.2 ml of HCl, and heated at 99°C for 30 minutes. The solution was then neutralised with NaOH, diluted 200-fold in 10 mM ammonium acetate, pH 7.5 and fractionated on a 75 ml Source 30Q column pre-equilibrated in 10 mM ammonium acetate pH 7.5 on a 10-column volume gradient of 10 mM to 500 mM ammonium acetate pH 7.5. Eluate was monitored at 218, 254 and 280 nm. Samples of fractions with

high 218 nm absorbance but negligible absorbance at the higher wavelengths containing the muropeptides of interest were diluted into 50% (v/v) acetonitrile and analysed by negative ion nano-spray time-of-flight mass spectrometry (**S.1.2.3.1.**). Muropeptides were freeze-dried thrice against water, and resuspended for storage at -20°C to a final concentration of 0.2 M

S.1.2.5. Preparation of non-polymerisable donor substrate analogue methylene lipid II-Lys.

A UDP-GlcNAc analogue (((3R,5R,6R)-3-acetamido-4,5-dihydroxy-6-(hydroxymethyl) tetrahydro-2H-pyran-2-yl)methyl) phosphonic ((5-(2,4-dioxo-3,4-dihydropyrimidin-1(2H)-yl)-3,4-dihydroxy tetrahydrofuran-2-yl) methyl phosphoric) anhydride (UDP:CH_2:GlcNAc) where the oxygen atom between the β-phosphorus of the UDP group and the C1 of the GlcNAc pyranose ring was replaced by a methylene was synthesised by GVKBio (Hyderabad, India). Methylene lipid II-Lys was synthesised from UDP:CH_2:GlcNAc in three steps:

UDP:CH_2:GlcNAc to UDP:CH_2:MurNAc. In a final volume of 8 ml, 2.84 mM UDP:CH_2:GlcNAc was incubated in 50 mM HEPES, 10 mM $MgCl_2$, 1 mM dithiothreitol, 9.1 mM phospho*enol*pyruvate, 50 mM KCl, 66.3 μM *E. coli* MurA, 3.45 μM *P. aeruginosa* MurB, 0.2 mM $NADP^+$, 1.125 $U.ml^{-1}$ isocitrate dehydrogenase and 26.5 mM *D*,*L* isocitrate, overnight at 37°C. Proteins were then removed by centrifugal ultrafiltration through a Viva Spin centrifugal concentrator with a 10,000 molecular weight cut-off at 4°C and 4,000 x g. The filtrate was diluted four fold into 10 mM ammonium acetate pH 7.5 and loaded onto a 75 ml column of Source 30Q anion exchange resin equilibrated in the same buffer. The column was washed at 10 $ml.min^{-1}$ in 10 mM ammonium acetate and UDP:CH_2:MurNAc was eluted in a 10 column volume gradient comprising 10 mM to 500 mM ammonium acetate, pH 7.5. Fractions containing UDP:CH_2:MurNAc were combined, desalted by freeze drying thrice and characterised by nanopsray mass spectrometry: Expected/found m/z (m-1)/1 and (m-2)/2 = 676.12/676.13 and 337.55/337.56 respectively. Recovery determined spectrophotometrically at 260 nm (uridine $\varepsilon_{260\ nm,\ 1\ cm}$ = 10,000 $M^{-1}.cm^{-1}$**[S12]**), was 10.9 μmol; 48%.

UDP:CH_2:MurNAc to UDP:CH_2:MurNAc-*L*-alanyl-γ-*D*-glutamyl-*L*-lysyl-*D*-alanyl-*D*-alanine. In a final volume of 4 ml, 2.73 mM UDP:CH_2:MurNAc was incubated in 50 mM HEPES, 10 mM $MgCl_2$, 1 mM dithiothreitol, 200 mM phospho*enol*pyruvate, 6 mM ATP, 5.53 $U.ml^{-1}$ (manufacturer's unit definition) rabbit muscle pyruvate kinase, 50 mM KCl, 15.2 μM *P. aeruginosa* MurC, 35 mM *L*-alanine, 13.8 μM *P. aeruginosa* MurD, 35 mM *D*-glutamate, 3.92 μM *S. pneumoniae* MurE, 35 mM *L*-lysine, 4.16 μM *S. pneumoniae* MurF and 35 mM *D*-alanyl-*D*-alanine, overnight at 37°C. The incubation was then subjected to centrifugal ultrafiltration and anion exchange chromatography as for the isolation of UDP:CH_2:MurNAc, to purify the UDP:CH_2:MurNAc-*L*-alanyl-γ-*D*-glutamyl-*L*-lysyl-*D*-alanyl-*D*-alanine product. Fractions containing the UDP:CH_2:MurNAc pentapeptide were desalted by freeze drying thrice and characterised by nanopsray mass spectrometry: Expected/found m/z (m-1)/1, (m-2)/2 and (m-3)/3 = 1146.37/1146.39, 572.68/ 572.68 and 381.45/381.46 respectively (Table S1). Overall recovery was 10.1 μmol; 44.4%.

UDP:CH_2:MurNAc-*L*-alanyl-γ-*D*-glutamyl-*L*-lysyl-*D*-alanyl-*D*-alanine to methylene lipid II-Lys. Undecaprenyl phosphate was resuspended to 1.35 mM in 3.5 ml of 0.1 M Tris, 5 % (v/v) Triton X-100, 5 mM $MgCl_2$, 2 mM UDP:CH_2:MurNAc-*L*-alanyl-γ-*D*-glutamyl-*L*-lysyl-*D*-alanyl-*D*-alanine, 6 mM UDP-GlcNAc, 0.07 $mg.ml^{-1}$ *E. coli* MurG and 5.26 mg (protein).ml^{-1} *Micrococcus flavus* membranes and incubated overnight at 37°C. The incubation was supplemented by 3.5 ml of pyridinium acetate pH 4.5 and 7 ml of water-saturated n-butanol and centrifuged at 4°C at 3,000 x g for 10 minutes. The upper phase was washed with 14 ml of water, recentrifuged at 4°C and 3,000 x g for 10 minutes, dried by rotary evaporation under vacuum, and the residue was resuspended in chloroform:methanol:water 2:3:1. Methylene lipid II-Lys was then purified by anion exchange chromatography and analysed by thin layer chromatography as described[S7]. Methylene lipid II-Lys was freed from ammonium bicarbonate by freeze drying thrice against water and resuspended in chloroform:methanol: water 2:3:1. Nanopsray time of flight mass spectrometry gave: expected/found m/z (m-1)/1,

(m-2)/2 and (m-3)/3 = 1872.07/1872.07, 935.53/935.54 and 623.35/623.36 respectively (Table S2; Figure S2). Overall recovery determined as described[S7] was 0.68 μmol; 6.7%.

S.1.2.6. Coupling enzyme assays

All assays were carried out at 30°C. Activity is defined as turnover (min^{-1}) or units where 1 μmole substrate converted or product formed per minute is 1 unit.

S.1.2.6.1. *R. gracilis D* amino acid oxidase activity. The enzyme was diluted 1 in in 10,000 into 50 mM Tris, 50 mM lactitol, 10% (v/v) glycerol and 5 mM EDTA, pH 7.5 prior to assay. Assays contained 50 mM *bis*-Tris propane, adjusted to pH 8.5, 20 mM $MgCl_2$, 0.1% (v/v) Triton X-100, 22.5-35 U (Manufacturer's definition).ml^{-1} rabbit muscle *L*-lactate dehydrogenase, 0.3 mM NADH and 1.25 nM *D*-amino acid oxidase. Auto-oxidation of NADH was followed for 5 minutes at 340 nm, after which time, D-amino acid oxidase activity was initiated by the addition of 1 mM *D*-alanine. The unit concentration of *D*-amino oxidase was derived from its initial rate which was calculated from the difference between rates in the presence and absence of 1 mM *D*-alanine ($\varepsilon_{1cm,\ 340\ nm}$ = 6,220 $M^{-1}.cm^{-1}$) [S12].

S.1.2.6.2. *E. coli* alanine racemase activity. The enzyme was diluted 1 in 10,000 from an 8.04 mM stock into alanine racemase storage buffer (**S.1.2.2.5**) prior to assay. Assays contained 50 mM *bis*-Tris propane, adjusted to pH 8.5, 20 mM $MgCl_2$, 36.1$U.ml^{-1}$ *R. gracilis D* amino acid oxidase, 14.3 $U.ml^{-1}$ horse radish peroxidase, 50 μM amplex Red and 20.1 nM alanine racemase. Any amino acid independent change in absorbance at 555 nm was followed after which time, alanine racemase activity was initiated by the addition of 0.1 mM *L*-alanine. The unit concentration of alanine racemase was derived from its initial rate which was calculated from the difference between rates in the presence and absence of 0.1 mM *L*-alanine (Resorufin $\varepsilon_{1cm,\ 555\ nm}$ = 54,000 $M^{-1}.cm^{-1}$)[S22].

S.1.2.6.3. Horse radish peroxidase Activity. The enzyme was diluted 1 in 400,000 into 50 mM *bis*-Tris propane pH 8.5 prior to assay. Assays contained 50 mM *bis*-Tris propane pH 8.5, 20mM $MgCl_2$, 50 μM amplex red, and 18.5 pM HRP. The absorbance at 555 nm was monitored

for two minutes, at which point, 20 μM hydrogen peroxide was added to initiate the assay. The unit concentration of HRP was derived from its initial rate which was calculated from the difference between rates in the presence and absence of hydrogen peroxide (Resorufin $\varepsilon_{1cm,\ 555\ nm}$ = 54,000 $M^{-1}.cm^{-1}$)[S22].

S.1.2.7. Monofunctional transglycosylase assays

SDS-PAGE assay of transglycosylase glycan products was based on the methods of Helassa *et al.*[S23] and Barrett *et al.*[S24]. In a final volume of 15 µl, 32.5 µM Lipid II $^{\varepsilon}$N-dansyl-Lys and 32.5 µM lipid II-Lys was resuspended in 20 mM Tris pH 8.0, 10 mM $MgCl_2$, 20% (v/v) DMSO, 0.05% (v/v) octa ethylene decyl ether and incubated with 5 μM *S. aureus* monofunctional transglycosylase at 20°C for 1 hour. Reactions were terminated with 0.5 mM moenomycin and incubated at 60°C for ten minutes at which point samples were centrifuged at 13,000 rpm to remove precipitated protein. Six-times Loading buffer was added (1 x loading buffer was 16.7 mM Tris pH 8.8, 0.67% (w/v) SDS, 6.7% (v/v) glycerol and 0.005% (w/v) bromophenol blue). Glycan chains were fractionated by SDS PAGE according to[S24] where samples were loaded without heat denaturation. Gels were run in anode buffer (0.1 M Tris, pH 8.8) and cathode buffer (0.1 M Tris, 0.1 M Tricine, 0.1% (w/v) SDS, pH 8.25) at 100 V and 50 mA for 1 hour and imaged by UV (302 nm) transillumination with a 516-600 nm filter using a Syngene GeneSnap G:Box Gel Doc (Syngene).

S.1.2.8. Global non-linear regression analysis of *E. coli* PBP1B transpeptidation kinetics

Replicate data sets of v_o *versus* [MurNAc *meso*-DAP tripeptide] were fitted to a rapid random equilibrium model (Equation 3, main text) and to equations for ordered rapid equilibrium mechanisms with lipid II-Lys (LII) or MurNAc *meso*-DAP tripeptide (M3P) as the leading substrate (Equations S2 and S3). The data was additionally fitted to a Ping Pong mechanism (Equation S4).

$$v_o = \frac{V_{max}.[LII].[M3P]}{K_{LII}.K_{M3P} + K_{M3P}.[LII] + [LII].[M3P]}$$ Equation S2

$$v_o = \frac{V_{max}.[LII].[M3P]}{K_{LII}.K_{M3P} + K_{LII}.[M3P] + [LII].[M3P]}$$ Equation S3

$$v_o = \frac{V_{max}.[LII].[M3P]}{K_{M3P}.[LII] + K_{LII}.[M3P] + [LII].[M3P]}$$ Equation S4

Data were treated as triples (x_i, y_i, z_i) (i = 1, …, N) consisting of the concentrations of lipid II-Lys (x) and MurNAc *meso*-DAP tripeptide (y) in µM, together with the corresponding reaction rate v_0 (z) (min^{-1}). In this way all data could be incorporated into the fitting. Equations 3, S2-S4 were therefore considered to corresponded to a surface, $z = f_k(x, y)$ (k = Equations 3, S2-S4), to be fitted to these data. Surface fitting was done using the *Curve Fitting Toolbox* in MATLAB 2017a (Mathworks) using robust nonlinear least squares (bisquare weights method) and the Trust-Region search algorithm recommended by the authors of the programme.

Nonlinear least squares seeks to determine the parameters that minimise the sum of squared errors (*SSE*) between data and model (surface) corresponding to

$$SSE = \sum_{i=1}^{N} w_i \left(z_i - f_k(x_i, y_i) \right)^2$$ Equation S5

where f_k corresponds to a particular choice for the reaction equation and w_i are weights used to adjust the contribution to the sum of different data points. Least squares fitting can be unduly influenced by the presence of outliers and so robust least squares was employed using *bisquare weights*, which weights (penalises) each data point (w_i, i = 1, …, N) according to how close the point is to the fitted surface.

In order to ensure that fits represented a global minimisation of the *SSE* the starting values for the parameters were varied. To provide starting fits for each of the equations 10,000 random starting points were used; each starting point was constructed by sampling an α (when applicable) from a uniform distribution from 0 to 1, and then K_{LII}, K_{M3P} and V_{max} each from a

uniform distribution on the logarithm of the parameter from 10^{-6} to 10^{+6}. These starting fits were further refined by randomly selecting 1,000 starting points from a uniform distribution on the logarithm of the parameters from 0.1 times to 10 times the current best estimate (except α which was sampled from a uniform distribution from 0 to 1).

The *SSE* value (and the corresponding root mean squared error, RMSE) was used as the primary goodness-of-fit measure across the four candidate equations. However, the random rapid equilibrium equation (equation 3) contains the remaining equations S2-S4 as nested special cases and therefore has an extra parameter. To compare the fits between equations 3, S2 and S3, an adjusted r^2 metric was used, which takes into consideration the extra degree of freedom afforded by the extra parameter.

S.2: Supplementary Results

S.2.1. Synthesis of *E.coli* PBP1B substrates and substrate analogues

Donors were synthesised in two stages. Firstly the UDP MurNAc pentapeptide precursor was generated and purified by anion exchange chromatography. All UDP MurNAc pentapeptide precursors were then characterised by high resolution FPLC anion exchange chromatography on a MonoQ 5/5 anion exchange column (bed volume 0.98 ml) eluted with a 0.01 to 1 M ammonium acetate gradient at 1 ml/minute. Elution of all UDP MurNAc precursors followed at 254 nm indicated on peak integration purities in excess of 95%. Negative ion time of flight mass spectrometry confirmed the synthesis of all UDP MurNAc precursors used herein to generate PBP1B donors and acceptors (Table S1). Lipid-linked donors, lipid-linked acceptors and analogues thereof were analysed by thin layer chromatography as described[S7] and were found to be chromatographically homogeneous, and gave the expected m/z values for singly, doubly or triply charged states on analysis by negative ion time of flight mass spectrometery (Table S2, Figure S1 and S2).

MurNAc *meso*-DAP tri, tetra and pentapeptide acceptors (both amidated and unamidated) were purified as single species by anion exchange chromatography. Synthesis of all molecules was confirmed by negative ion time of flight mass spectrometry (Table S2 and Figure S2). Analysis of all MurNAc peptide acceptors with the exception of MurNAc *meso*-DAP tetrapeptide-NH_2 revealed a small amount of in source fragmentation (Figure S2) to yield the corresponding lactyl peptides (marked as (m-1H^+)/1 –GlcNAc; Figure S2). This was a feature shared with all of the transpeptidation and carboxypeptidation products analysed by LCMS in positive ion mode, which irrespective of retention time, always apparently co-chromatographed with detectable but negligible amounts of their corresponding lactyl peptide from which loss of GlcNAc was observed.

S.2.2. LCMS and LCMSMS analysis of PBP1B transpeptidase and carboxypeptidase products

S.2.2.1. Lipid II-*meso*-DAP and lipid II-*L*,*L*-DAP transpeptidation products. Analysis of transpeptidation products formed from lipid II-*meso*-DAP detected elution of three closely eluting anomeric species (Figure 2c) with a m/z consistent with that of the doubly charged molecule anticipated (Figure 2a) on muramidase digestion of the PBP1B product ((m+2)/2 = 966.92). LCMSMS collision induced fragmentation of all three peaks yielded an identical fragmentation pattern where all ions were singly charged (Figure 2d). Ions 1-19, 22, 24, 27-32, 36, 37 and 41 were all transpeptidation products with m/z values consistent with *D*,*D* 4,3 transpeptidation with a peptide bond formed between the donor fourth position *D*-alanyl α-carbonyl and the acceptor third position *meso*-DAP ε-amino group (Table S3). All other ions were fragments with m/z values originating from either the donor or acceptor but not encompassing the transpeptidation linkage itself. Ions 1-7, 10-12, 14-16, 19-21, 23, 25 and 32 were fragments from which one or two water molecules had been lost either from the MurNAc sugars or the lactyl group (Table S3).

For the majority of ions with acceptor and donor fragments linked by transpeptidation, MSMS analysis, although definitive about the presence of a structure generated by

transpeptidation were otherwise ambiguous. In these instances m/z values were consistent with loss of equivalent residues from either the donor or the acceptor (Fragments 4-8,11-15, 17-19 and 22, 29; Table S3).

The anticipated Lipid II-*L*,*L*-DAP derived transpeptidation product (identical in structure to that in Figure 2a, except that ε-carbon atom stereocentre of DAP residues were in the L-configuration), was formed in much lower abundance than that from transpeptidation of lipid II-*meso*-DAP (Figure 4a). Extracted ion chromatogram peaks for this species (expected (m+2)/2 = 966.92) revealed three anomerically related peaks with elution times of 7.62, 7.34 and 7.05 minutes respectively. Fragmentation of the 7.62 minute species by MSMS (Figure S11a) was identical to that of 966.92 m/z ions eluted at 7.34 and 7.05 minutes respectively and revealed a pattern of ions virtually identical to those observed for fragmentation of lipid II-*meso*-DAP (Table S3). The only significant difference between the fragmentation patterns derived from lipid II-*L*,*L*-DAP and lipid II-*meso*-DAP was that the lower abundance of the former raised the prominence of contaminating ions such as 283.19 ((m+1/1); Figure S11a).

S.2.2.2. LCMSMS analysis of the carboxypeptidation product of lipid II-*meso*-DAP and lipid II-*L*,*L*-DAP

LCMS analysis of the products of PBP1B catalysis revealed that turnover of lipid II-*meso*-DAP and lipid II-*L*,*L*-DAP substrates both yielded species with m/z values consistent with a disaccharide tetrapeptide structure (Figure 2b) generated by substrate carboxypeptidation (Figure 4b and Figure S3aii and bii). These molecules fractionated identically by LCMS, each eluting as two anomer peaks at 7.45 and 7.10 minutes for the *meso*- and *L*,*L*-DAP disaccharide tetrapeptides derived from lipid II-*meso*-DAP and lipid II-*L*,*L*-DAP (Figure 2c; disaccharide *meso*-DAP tetrapeptide shown).

In order to confirm the structure of these singly charged 940.40 m/z species, they were subjected to LCMSMS, yielding mass spectra corresponding to fragments of the species (Table S4) derived from carboxypeptidase activity arising from lipid II-*meso*-DAP *and* lipid II-

L,*L*-DAP utilization (Figures S3ai and bi respectively). Both fragmentation spectra contained identical fragments where the poorer abundance of fragment ions for the disaccharide *meso*-DAP tetrapeptide (Figure S3ai) compared to that of the disaccharide *L*,*L*-DAP tetrapeptide (Figure S3bi) was consistent with the lower rate of carboxypeptidation by PBP1B of *meso*-DAP-containing stem peptides relative to *L*,*L*-containing stem peptides (Figure 4b). Both fragmentation patterns were interpretable as being derived from a molecule with the predicted structure generated by *D*,*D*-carboxypeptidation (Figure 2b).

For both *meso*- and *L*,*L*-DAP tetrasaccharide peptides, fragmentation (Table S4) of the 940.40 m/z species eluting at 7.45 minutes was accompanied by loss of water (ions 2, 4-7 and 9), loss of the GlcNAc moiety (ions 3-15 and 17) which appeared as a fragment in its own right (ion 16), loss of the MurNAc moiety (Fragments 8-15 and 17) and principally sequential fragmentation from the N-terminal end of the peptide (ions 10, 12 and 15) with additional loss of the C-terminal *D*-alanine (ions 11, 13 and 14). Consequently, both fragmentation patterns were entirely consistent with the proposed structure of the disaccharide *meso*- and *L*,*L*-DAP tetrapeptide products. Identical fragmentation patterns were observed for both anomers of the *meso*- and *L*,*L*-DAP tetrasaccharide peptides eluting at 7.10 minutes.

S.2.2.3. LCMSMS Analysis of the transpeptidation product of lipid II-Lys and MurNAc *meso*-DAP pentapeptide

LCMS analysis of transpeptidation products formed from lipid II-Lys and MurNAc *meso*-DAP pentapeptide detected elution of three closely eluting anomerically related species at 7.53, 7.28 and 6.98 minutes (Figure S4b) with a m/z consistent with that of the doubly charged molecule anticipated (Figure S4a) on muramidase digestion of the PBP1B product (Observed (m+2)/2 = 843.38; all peaks, expected: 843.38).

LCMSMS (Figure S4c) of the 843.38 species eluting at 7.53 minutes yielded fragments that could only be interpreted in terms of an acceptor peptide strand (or N-terminal truncations thereof) linked through the ε-amine of *meso*-DAP to the α-carbonyl of the *D*-alanyl

residue donor strand originating from lipid II-Lys. These corresponded to fragment ions in Table S5 listed as 1 to 26, 28, 29, 31, 32, 34, 36, 37, 39, 45, 47, 50 and 53.

Although these ions represented fragments of donor and acceptor strands linked by transpeptidation, in many cases the m/z values could be represented by more than one structure resulting from transpeptidation, both consistent with the structure of the presumptive transpeptidation product (Figure S4a), depending upon whether loss occurred through fragmentation of the donor or the acceptor strand (fragments 1, 2, 4, 5, 6, 8, 11, 13, 15, 19-26 29, 31, 32, 36, and 39; Table S5, Figure S4c).

All other fragments were either derived solely from the donor or acceptor strand, or were ambiguous in that they couldn't be represented by structures uniquely consistent transpeptidation (fragments 38, 40, 49, 56; Table S5). Fragmentation of species derived from the transpeptidase donor containing GlcNAc:MurNAc disaccharides (1), or containing donor and acceptor fragments with N-terminal lactyl or muramyl moieties (4,7,8,10, 11, 15-18, 20, 22 and 25; Table S5) was often characterised by (sometimes multiple) loss of water.

Fragmentation of the other anomer 843.38 m/z species eluting at 7.28 and 6.98 min yielded mass spectra which were identical to that of the ions eluting at 7.53 min confirming that the 843.38 species in each peak were likely to be identical.

S.2.2.4. LCMSMS Analysis of the carboxypeptidation product of lipid II-Lys

Analysis of PBP1B catalysis with lipid II-Lys alone revealed that PBP1B could truncate the stem peptide of lipid II-Lys through *D*,*D*-carboxypeptidation as revealed spectrophotometrically although the rate was much less than that of transpeptidation (Figure 1e and f). Nevertheless, a species indicative of lipid II-Lys carboxypeptidation, with a m/z of 896.41 (expected for disaccharide lys tetrapeptide ($m+1H^+$)/1= 896.41) (Figure S5a) was easily detectable by LCMS (Figure S5b and c). The 896.41 species eluted as two (presumably anomerically related) species with retention times of 6.41 and 5.89 minutes.

In order to confirm the structure of these singly charged 896.41 m/z species in the LCMS 6.41 minute peak, these ions were subjected to LCMSMS, yielding mass spectra (Figure S5d) containing fragments of the 896.41 species (Table S6).

Fragmentation (Table S6) was accompanied by loss of water (ions 2, 4-6, 8, 11,12 and 16), loss of the GlcNAc moiety (ions 3-6) which appeared as a fragment in its own right (ion 18), loss of the MurNAc moiety (ions 7,8,10,11) which appeared as a fragment in its own right (ion 16) and sequential fragmentation from the N-terminal end of the peptide (ions 13, 15 and 17) with additional loss of the C-terminal *D*-alanine (ions 10, 14 and 15). The fragmentation pattern also contained ions suggestive of intact loss of the disaccharide (ion 9), additionally with deacetylation (ion 12). LCMSMS analysis of the m/z = 896.41 species eluting at 5.89 minutes generated mass spectra that were super-imposible over that in Figure S5a. Consequently, both fragmentation patterns were entirely consistent with the proposed structure of the disaccharide Lys tetrapeptide structure (Figure S5a) generated by *D*,*D*-carboxypeptidation of lipid II-Lys.

S.2.2.5. LCMSMS Analysis of the transpeptidation product of lipid II-*L*,*L*-$^{\varepsilon}$NAc.DAP and MurNAc *meso*-DAP pentapeptide

The doubly charged cation $(m+2H^+)/2$ = 886.38 of the transpeptidation product of PBP1B with a lipid II-*L*,*L*-$^{\varepsilon}$NAc.DAP donor and a MurNAc *meso*-DAP pentapeptide (Figure 4c) eluted as three anomer peaks at 8.21, 8.02 and 7.86 minutes on LCMS. Fragmentation of the 8.21 minute 886.38 species yielded singly charged fragments (Figure S11b) corresponding to the structures that could only be interpreted in terms of an acceptor peptide strand (or N-terminal truncations thereof) linked through the ε-amine of *meso*-DAP to the α-carbonyl of the D-alanyl residue donor strand originating from lipid II-*L*,*L*-$^{\varepsilon}$NAc.DAP. These corresponded to fragment ions in Table S7 listed as 1 to 8, 10, 12, 14, 15, 17, 18, 20, 33 and 38).

Although these ions represented fragments of donor and acceptor strands linked by transpeptidation, in many cases the m/z values could be represented by more than one

structure consistent with the structure of the presumptive transpeptidation product, depending upon whether loss occurred through fragmentation of the donor or the acceptor strand (fragments listed as 1 to 8, 12, and 14; Table S7). All other fragments were either derived solely from the donor or acceptor strand, or were ambiguous in that they couldn't be represented by structures uniquely consistent with transpeptidation (fragments 25, 26, 30, 34). Fragmentation of species derived from the transpeptidase donor containing N-terminal lactyl or muramyl moieties was often characterised by (sometimes multiple) dehydration (fragments listed as 1-3, 8, 9,11,13,14,16,18, 22, 24, 26, 28, 31, 37, 42; Table S7).

Fragmentation of 886.38 m/z species eluting at 8.02 and 7.86 min yielded mass spectra which were identical to that of the ions eluting at 8.21 minutes to the extent that all three fragmentation spectra were superimposible, confirming that the 886.38 species in each peak were likely to be identical.

S.2.3. Global non-linear least sqauares analysis of the impact of donor on the dependence of PBP1B on acceptor.

Table S8 shows the fitted parameters and the corresponding goodness-of-fit measures for the four equations (3: random rapid equilibrium, S2: ordered rapid equilibrium, donor first; S3: ordered rapid equilibrium acceptor first and S4, Ping Pong). Comparison of the sum of squared errors (SSE) for fits to equations with the same number of parameters (equations S2-S4) suggested that the ordered rapid equilibrium equation S2 (lipid II-Lys before MurNAc *meso*-DAP tripeptide) provided the best fit for the equations involving three parameters. However, the random rapid equilibrium equation (3) had the smallest SSE and provided the closest fit to the data.

Since Equation S2 is a nested case relative to Equation 3, the adjusted-r^2 gives a measure between the two equations that can be used for comparing them. However, both the SSE and adjusted-r^2 values were similar for the two equations (Table 8) making it difficult to definitively determine whether equation 3 or equation S2 fitted the data preferentially and

therefore whether the data were best fitted to a rapid random or ordered equilibrium mechanism. Consistant with this, fitting the data to equations 3 and S2 generated values for the kinetic constants that are plausible in the context of the concentration ranges of LII and M3P employed and the dependences of v_o on M3P observed (Table S8, Figure S13 , Figure 5h).

An ordered rapid equilibrium mechanism can be distinguished from a random equilibrium mechanism if both substrates are in large excess of enzyme (as in Figure 5 where; [PBP1B] = 0.0096 μM, [Lipid II-Lys] = 5-60 μM, [MurNAc *meso*-DAP tripeptide] = 7.5-80 μM). In this case, for an ordered mechanism, at saturating concentrations of the substrate that binds second, the equilibrium of the binding of the first substrate to the free enzyme would be pulled to complete conversion of free enzyme to the first substrate:enzyme complex and therefore V_{max} would be independent of the concentration of the first substrate that binds in this mechanism[S25]. Consequently, a double reciprocal plot of $1/v_o$ vs 1/[second substrate], at various constant first-binding substrate concentrations, would have a common intercept of $1/V_{max}$ on the $1/v_o$ axis[S25]. This is not the case for a random rapid equilibrium mechanism, where for both substrates, apparent V_{max} values for one substrate increase hyperbolically with varying constant concentrations of the other substrate[S26] and consequently, plots of $1/v_o$ vs. 1/[substrate A or B] at various constant [substrate B or A] intersect behind the $1/v_o$ axis[S26]

Reference to Figure 5 in the main manuscript shows the anticipated intersections of double reciprocal plots of fits to both equations S2 and 3, where as expected from the above, fitted lines intersect behind[26] (equation 3, Figure 5g) or on[S25] (equation S2, Figure 5f) the $1/v_o$ axis. The x-axis co-ordinate of point of intersection of the double reciprocal plots of fits to equation 3 is $-1/K_{M3P}$[S26]. As global fitting to equation 3 yielded a K_{M3P} =130 ± 80 μM (Table S8), the intersection x-axis co-ordinate in Figure 5g was -0.0077, very close to the $1/v_o$ axis, which underpins the difficulty in statistically discriminating between the random and ordered mechanisms (equations 3 and S2) with the available data.

Parameter estimates for equation S3 were quite poorly defined (Table S8) and when combined with the goodness-of-fit measures strongly suggest that this equation is a poor choice given the available data. Considering comparison of fits of equation 3 (random) and S3 (ordered, M3P first), a double reciprocal plot of $1/v_o$ vs 1/[M3P] for equation S3 would be expected to generate a family of lines at several constant [LII] values intersecting behind the $1/v_o$ axis with an x co-ordinate of $-1/K_{M3P}$[S25]. However, inspection of Figure 5d, shows this intersection to be apparently on the $1/v_o$ axis. Although this would appear to be counter to what would be anticipated for this mechanism, it was not. K_{M3P} was *very* poorly defined in the fit of the data to equation S3 with a fitted value of 100,000 ± 30,000,000 μM (Table S8). As $-1/K_{M3P}$ for the fit of data to equation S3 was -0.00001, the double reciprocal plot point of intersection was mathematically distinct from, but practically (visually) indistinguishable from intersection on the $1/v_0$ axis (Figure 5d).

The constants that result from fitting of data to equation S3 were inconsistent with the experimental data and prone to exceptionally high error. For example, our experimental data (Figure 5h, Figure S13) show that in all cases, v_o vs [M3P] relationships are approaching saturation by 80 μM which was completely inconsistent with a fitted value of K_{M3P} of 100,000 μM. Finally, the error of this particular fit was far poorer as estimated by sum of squared errors (Table S8) than that of fits to equations 3 and S2, and cannot be considered to be reliable. These considerations led to rejection of equation S3 as a description of the mechanism employed by PBP1B transpeptidation.

Finally, equation S4 could be discounted on inspection of SSE estimates (Table S8) as is also clear from Figures 5e and S13, eliminating a Ping Pong mechanism as the kinetic scheme obeyed by *E.coli* PBP1B transpeptidation.

S.3: Supplementary Table Legends

Table S1: Observed and expected m/z values on mass spectrometric analysis of UDP precursors of PBP1B substrates and inhibitors. Samples were freed from ammonium acetate remaining after purification of the UDP precursors by lyophilisation, suspended in water, and analysed by negative ion mode nano-spray time of flight mass spectrometry (**S.1.2.3.1**). Combined scans were collected, converted to mass spectra using Mass Lynx software (Waters Ltd) and the m/z values observed for singly, triply and doubly charged states were compared to their corresponding expected values.

Table S2: Observed and expected m/z values on mass spectrometric analysis of PBP1B donors and acceptors and analogues thereof. 100-500 pmol of each lipid I and lipid II species or derivatives thereof were dried down in a glass vial and resuspended in 0.1 ml of 70% (v/v) methanol and 7.5 mM ammonium acetate. All other analytes were resuspended between 1 and 5 μM in 50% (v/v) acetonitrile. Samples were then analysed as described in the legend to Table S1.

Table S3: Identification of MSMS collision-induced fragment ions of PBP1B transpeptidation products derived from lipid II-*meso*-DAP and lipid II-*L*,*L*-DAP. Assays were carried out in the presence of either 20 μM lipid II-*meso*-DAP or 20 μM lipid II-*L*,*L*-DAP and 9.54 nM *E. coli* PBP1B and analysed by LCMSMS (**S.1.2.3.2.1**). Survey chromatograms (LCMS) identified elution of ions as a series of three anomeric peaks with an m/z value identical to that of the doubly charged transpeptidation product derived from either lipid II-DAP stereoisomer (expected/observed (m+2H)+/2 = 966.92/966.91) eluting at 7.92, 7.65 and 7.31 minutes (Main manuscript Figure 2a,c); lipid II-*L*,*L*-DAP data not shown). Transpeptidation product ions were then fragmented by collision-induced dissociation (Figure 2d). Mass spectra of the fragmented ions of transpeptidation products derived from lipid II-*meso*-DAP and lipid II-*L*,*L*-DAP eluting at 7.92 minutes were extracted by the Mass Lynx software package. Fragments in Table S3 with the transpeptidation intact are denoted by a purple number with a yellow square surround. All fragments that no longer contain this linkage are denoted by a

yellow number with a purple square surround. Donor peptides are rendered in blue, acceptor peptides are green. Un-crosslinked peptide fragments, that originated from either donor or the acceptor are rendered gray. All fragments were singly charged. The fragmentation patterns for the anomers of the *L*,*L*- or *meso*-DAP transpeptidation products eluting at 7.65 and 7.31 minutes were superimposable over the corresponding 7.92 minute data.

Table S4: Identification of MSMS collision-induced fragment ions of PBP1B carboxypeptidation products derived from lipid II-*meso*-DAP and lipid II-*L*,*L*-DAP. Assays were carried out in the presence of either 20 μM lipid II-*meso*-DAP or 20 μM lipid II-*L*,*L*-DAP and 9.54 nM *E. coli* PBP1B and analysed by LCMSMS (**S.1.2.3.2.1**). Survey chromatograms of analysis of products derived from both lipid II-*meso*-DAP or lipid II-*L*,*L*-DAP (LCMS) identified elution of two (presumably) anomer peaks of ions eluting at 7.45 min and 7.10 min (Figure 2c, trace (ii) for lipid II-*meso*-DAP shown) with a m/z value identical to that of the singly charged carboxypeptidation product (expected (m+1H)+/1 = 940.40), which were then fragmented by collision-induced dissociation (Figure S3). The resulting MSMS spectra for each anomeric peak of the carboxypeptidation products derived from lipid II-*meso*-DAP and lipid II-*L*,*L*-DAP were superimposable and the fragment ions of the major 7.45 minute peak for the carboxypeptidation product derived from both lipid stereoisomers are recorded in this table. All fragments are denoted by a yellow number with a purple square surround. Donor peptides are rendered in blue as all originate from the donor (the acceptor is water).

Table S5: MSMS collision-induced fragment ions of PBP1B transpeptidation products derived from lipid II-Lys and MurNAc *meso*-DAP pentapeptide. Assays were carried out in the presence of 20 μM lipid II-Lys, 20 μM MurNAc *meso*-DAP pentapeptide and 9.54 nM *E. coli* PBP1B and analysed by LCMSMS (**S.1.2.3.2.1**).

Survey chromatograms (LCMS) identified elution of ions with an m/z value numerically identical to that of the doubly charged transpeptidation product (expected/observed $(m+2H^+)/2$ = 843.38/ 843.38) as three anomeric peaks at 7.53, 7.28 and 6.98 minutes (Figure S4(b)), which were then fragmented by collision-induced dissociation. Fragmentation mass spectra were identical for the 7.53, 7.28 and 6.98 minute peaks, and the data for the 7.53 minute peak is interpreted in Table S5 where branched peptides linked by transpeptidation are denoted by a purple number with a yellow square surround. All fragments that no longer contain this linkage are denoted by a yellow number with a purple square surround. Donor peptides are rendered in blue, acceptor peptides are in green. For many crosslinked peptides the observed m/z can be interpreted by either acceptor or donor peptide fragmentation (ions 1, 2, 5, 6, 8, 11, 13, 15, 19-26, 29, 31, 32, 36 and 39) although in all cases can only be interpreted as being crosslinked by transpeptidation. All fragments were singly charged.

Table S6: Identification of MSMS collision-induced fragment ions of PBP1B carboxypeptidation products derived from lipid II-Lys. Assays were carried out in the presence of 20 μM lipid II-Lys, 20 μM MurNAc *meso*-DAP pentapeptide and 9.54 nM *E. coli* PBP1B and were analysed by LCMSMS (**S.1.2.3.2.1**). Survey chromatograms (LCMS) identified elution of two peaks of ions at 6.41 minutes and 5.89 minutes with a m/z value corresponding to anomers of the singly charged carboxypeptidation product (expected (m+1H)+/1 = 896.41, observed m/z 896.41; Figure S5b,c), which were then fragmented by collision-induced dissociation (Figure S5d). All fragments are denoted by a yellow number with a purple square surround. Donor peptides are rendered in blue as all originate from the donor (the acceptor is water). Fragmentation patterns for the 6.41 minute and 5.89 minute peaks were identical, the 6.41 minute peak fragmentation pattern is interpreted in Table S6.

Table S7: MSMS collision-induced fragment ions of PBP1B transpeptidation products derived from lipid II-*L*,*L*-$^{\varepsilon}$NAc.DAP and MurNAc *meso*-DAP pentapeptide. Assays

were carried out in the presence of 20 μM lipid II-*L*,*L*-$^{\varepsilon}$NAc.DAP, 20 μM MurNAc *meso*-DAP pentapeptide and 9.54 nM *E. coli* PBP1B and were analysed by LCMSMS (**S.1.2.3.2.1**). Survey chromatograms (LCMS) identified elution of ions with a m/z value identical to that of the doubly charged transpeptidation product (expected/observed $(m+2H^+)/2$ = 886.38/ 886.38) as three anomeric peaks at 8.21, 8.02 and 7.86 minutes (Figure 4c), which were then fragmented by collision-induced dissociation. Mass spectra of the fragmented ions of all three peaks were identical and the data for the 8.21 minute peak is interpreted in Table S7 where branched peptides linked by transpeptidation are denoted by a purple number with a yellow square surround. All fragments that no longer contain this linkage are denoted by a yellow number with a purple square surround. Donor peptides are rendered in blue, acceptor peptides are in green. For many crosslinked peptides the observed m/z can be interpreted by either acceptor or donor peptide fragmentation (ions 1- 8, 12, and 14) although in all cases can only be interpreted as being crosslinked by transpeptidation. Un-crosslinked peptide fragments, that originated ambiguously from either the donor or the acceptor are rendered gray. All fragments were singly charged.

Table S8: Fitted values of kinetic constants and goodness-of-fit measures across the four different equations describing rapid equilibrium random, ordered and Ping Pong Mechanisms Equations 3 (main text), S2, S3 and S4 were fitted by Global least squares using MATLAB 2017a to the raw data in Figure 5h as described in **S.1.2.8.**

S.4: Supplementary Figure Legends

Figure S1: Nanospray Time of flight analysis of lipid II donors and analogues thereof modified at the second, third and fifth position of the pentapeptide stem.

Negative ion mass spectra were collected as described **S.1.2.3.1**. Charge states for singly, doubly and triply ionised molecules are denoted as (m-H^+)/1, (m-$2H^+$)/2 and (m-$3H^+$)/3 where in all cases the doubly charged species predominated, associated with sodiated species. All m/z values agreed with their expected values (Table S2).

Figure S2: Nanospray Time of flight analysis of inhibitors, acceptors and analogues thereof of *E. coli* PBP1B. Negative ion mass spectra were collected as described in **S.1.2.3.1**. Charge states for singly, doubly and triply ionised molecules are denoted as (m-H^+)/1, (m-$2H^+$)/2 and (m-$3H^+$)/3. All m/z values agreed with their theoretical expected values (Table S2). The MurNAc *meso*-DAP tri, tetra and pentapeptides and their amidated MurNAc *meso*-DAP tripeptide-NH_2 and MurNAc *meso*-DAP pentapeptide-NH_2 homologues were associated with varying amounts of in-source fragmentation upon analysis yielding small quantites of the associated lactyl peptides (denoted as –GlcNAc).

Figure S3: LCMS and LCMSMS of the PBP1B *D*,*D*-carboxypeptidation product derived from lipid II-*meso*-DAP and lipid II-*L*,*L*-DAP. Assays were carried out with either 20 μM lipid II-*meso*-DAP or 20 μM lipid II-*L*,*L*-DAP and 9.54 nM *E. coli* PBP1B and were analysed by LCMSMS (**S.1.2.3.2.1**). Survey chromatograms identified products derived from both lipid II-*meso*-DAP or lipid II-*L*,*L*-DAP (LCMS) with identical elution of two (presumably) anomer peaks of ions at 7.45 min and 7.10 min for each lipid II-DAP stereoisomer product (Figure 2c, trace (ii) for lipid II-*meso*-DAP shown) with m/z values identical to that of the singly charged carboxypeptidation product (either DAP isomer, expected (m+1H^+) /1 = 940.40, Figure S3(bii) (*L*,*L* lipid stereoisomer) and (aii) (*meso*-lipid stereoisomer) eluting at 7.45 minutes), which were then fragmented by collision-induced dissociation. The resulting MSMS spectra for each anomeric peak for the carboxypeptidation products derived from lipid II-*meso*-DAP and lipid II-*L*,*L*-DAP were superimposable and the fragment ions of the major 7.45 minute peak for carboxypeptidation of both *L*,*L* and *meso*-lipid stereoisomers are recorded in Figure

S3(ai) and (bi) respectively. All fragments are denoted by a yellow number with a purple square surround and are identified in Table S4.

Figure S4: LCMS and LCMSMS of the product of transpeptidation between lipid II-Lys and MurNAc *meso*-DAP pentapeptide. Assays were carried out with 20 μM lipid II-lys, 20 μM MurNAc *meso*-DAP pentapeptide and 9.54 nM *E. coli* PBP1B and analysed by LCMS and LCMSMS (**S.1.2.3.2.1**). **Panel (a)**: the putative transpeptidation product, where disaccharide tetrapeptide (donor, in blue) is crosslinked to the MurNAc *meso*-DAP pentapeptide (acceptor, green). **Panel (b)**: the extracted ion chromatograms for the elution of this transpeptidation product (expected $(m+2H^+)/2$ = 843.38) where the blue, red and purple chromatograms represents fractionation of the complete reaction, the reaction from which the MurNAc *meso*-DAP pentapeptide has been omitted and the reaction from which the donor lipid II-Lys has been omitted respectively. 843.38 m/z products were detected solely in the complete reaction and fractionated into three (presumably) anomer peaks of ions eluting at 7.53, 7.28 and 6.98 min. The mass spectrum for the 7.53 minute peak is shown (inset, expected = observed (m+2H)+/2 = 843.38). Identical mass spectra could be derived from the 7.28 and 6.98 minute peaks. **Panel (c)**: the mass spectrum of the fragmentation of the 843.38 m/z ion in the 7.53 minute peak. This fragmentation pattern was superimposable over that obtained from LCMSMS of the ions comprising the 7.28 and 6.98 minute peaks. All fragments that are linked by transpeptidation are denoted by a purple number with a yellow square surround and labelled with a yellow T in a green circle, whereas fragments that do not contain this linkage are denoted by a yellow number with a purple surround. Fragment numbering corresponds to the numbering of fragment structures in Table S5.

Figure S5: LCMS analysis of the impact of transpeptidation between Lipid II-Lys and MurNAc *meso*-DAP pentapeptide on the residual *D*,*D*-carboxypeptidase activity of PBP1B. Assays were carried and analysed by LCMS and LCMSMS exactly as described in the legend to Figure S4. **Panel (a)**: the structure of the putative

carboxypeptidation product. **Panel (b)**: the extracted ion chromatograms for the elution of this species (expected ($m+1H^+$)/1 = 896.41) where the purple, blue and red chromatograms represents fractionation of the complete reaction, the reaction from which the MurNAc *meso*-DAP pentapeptide acceptor has been omitted and the reaction from which the donor lipid II-Lys and MurNAc *meso*-DAP pentapeptide acceptor has been omitted respectively. Carboxypeptidation product of ($m+1H^+$)/1 = 896.41 eluted as two presumably anomeric species at 6.41 and 5.89 minutes where lipid II-Lys was present, but was markedly diminished by the presence of acceptor. **Panel (c)**: the mass spectrum for the 6.41 minute peak of elution of the carboxypeptidation product generated in the presence of donor alone (inset, expected (m+1H)+/1 = observed ($m+1H^+$) /1 = 896.41). Identical mass spectra could be derived from the 5.89 minute peak of this incubation. **Panel (d)**: the mass spectrum of the fragmentation of the 896.41 m/z ion in the 6.41 minute peak obtained from analysis of the reaction of PBP1B in the presence of donor and acceptor. This spectrum was superimposable over that obtained from LCMSMS of the ions comprising the 5.89 minute peak. All fragments are denoted by a yellow number with a purple square surround. Fragment numbering corresponds to the numbering of fragment structures in Table S6.

Figure S6: Transglycosylase activity of PBP1B and inhibition of transpeptidase activity by a non-polymerizable analogue of lipid II-Lys and hen egg white lysozyme. Panels (a) and **(b):** Transglycosylase assay of PBP1B activity as undecaprenyl phosphate release. For both panels, transglycosylase activity of 6.16 nM PBP1B was assayed in the presence of 20 μM lipid II-lys and 20 μM MurNAc *meso*-DAP tetrapeptide using negative ion nanospray time of flight mass spectrometry (**S.1.2.3.2.2**). % values correspond to the proportion of 2:1 isopropanol/methanol in the eluant of the Bond Elut CN-E reverse phase columns used to fractionate the lipid II-Lys substrate and undecaprenyl pyrophosphate in these assays. **Panel (a)**: the control

reaction where 10 μM moenomycin was added to the assay prior to addition of PBP1B, where elution of lipid II-Lys is observed between 40 and 60% (v/v) 2:1 isopropanol/methanol (Expected ($m\text{-}2H^+/2$) = 936.52; observed ($m\text{-}2H^+/2$) for 40, 50 and 60% washes = 936.53, 936.53 and 936.52 respectively). **Panel (b)**: the results of the experiment where 10 μM moenomycin was added to stop the reaction at the end of the assay. The lipid II-Lys ion is lost and the undecaprenyl pyrophosphate anion is prevalent in the 50, 60 and 70% (v/v) washes (Expected ($m\text{-}1H^+/1$) = 925.62 = observed ($m\text{-}1H^+/1$) for 50, 60 and 70% (v/v) washes). **Panel (c):** Inhibition of *E. coli* PBP1B transpeptidation through inhibition of transglycosylase activity by moenomycin. PBP1B (10 nM) transpeptidase was assayed with 40 μM lipid II-lys and 40 μM MurNAc *meso*-DAP pentapeptide. Moenomycin was added to the assay with the PBP for two minutes prior to addition of lipid II-Lys and MurNAc *meso*-DAP pentapeptide. Here, the assay was adapted to run in a low volume format (10 μl) employing resorufin fluorescence (Ex. 540 nm/Em. 590 nm) (Walkowiak[S27]). Data were plotted as % remaining activity vs a control omitting moenomycin and were fitted to the equation [S28]

$$\frac{v_i}{v_o} = 1 - \frac{\left([E] + [I] + K_i\left(1 + \frac{[S]}{K_m}\right)\right) - \sqrt{\left([E] + [I] + K_i\left(1 + \frac{[S]}{K_m}\right)\right)^2 - 4[E][I]}}{2[E]} \qquad \text{Equation S6}$$

Presuming competitive tight binding inhibition, where v_i and v_o are the inhibited initial rate and control no inhibitor rate respectively, [E], [S] and [I] are the concentrations of PBP1B, lipid II-Lys and moenomycin respectively, K_m is the apparent Michaelis constant for lipid II-Lys (35 ± 9 μM; Walkowiak[27] in this fluorescent low volume assay format) and K_i is the dissociation constant for moenomycin. Error bars are standard deviation (n=16). **Panel (d):** Structure of lipid II-Lys and methylene lipid II-Lys. The generic structure of the lysine variant of lipid II is drawn where, in lipid II-Lys, **R_1** is an oxygen wheras for methylene lipid II-Lys, **R_1** is a CH_2 moiety. **Panel (e)**: Evaluation

of the ability of methylene lipid II-Lys to act as a PBP1B transpeptidase donor. PBP1B (8.49 nM) transpeptidase was assayed with 20 μM methylene lipid II-Lys (**S.1.2.5.**) or lipid II-lys (positive control) and 20 μM MurNAc *meso*-DAP pentapeptide. Assays with both lipids were performed in triplicate. Error bars are standard deviation. **Panel (f)**: Evaluation of the ability of methylene lipid II-Lys to act as a PBP1B transpeptidase inhibitor. PBP1B (8.49 nM) transpeptidase was assayed with 4 μM lipid II-Lys and 20 μM MurNAc *meso*-DAP pentapeptide in the presence and absence of 16 μM methylene lipid II-Lys (**S.1.2.5.**) in triplicate or quintuplicate respectively. Error bars are standard deviation. **Panel (g)**: Inhibition of PBP1B transpeptidase activity by hen egg white lysozyme. PBP1B (8.49 nM) transpeptidase was incubated in triplicate with 20 μM lipid II-Lys in the presence or absence of hen egg white lysozyme for six minutes at which point residual transpeptidase activity was assayed by addition of 20 μM MurNAc *meso*-DAP pentapeptide.

Figure S7: Transpeptidase activity of *E. coli* PBP1B with polymerised and unpolymerizable donors and acceptors. **Panel (a)**: Impact of lipid II-Lys polymerization by *Staphylococcus aureus* monofunctional transglycosylase (MGT) on PBP1B transpeptidation. 20 μM Lipid II-Lys was added to a transpeptidase assay with (Trace **b**) or without (Trace **a**) 5.72 μM MGT. After two minutes PBP1B (8.62 nM) was added to either assay and at 8 minutes, the assays were supplemented with 20 μM MurNAc *meso*-DAP pentapeptide. Additionally, assays were run without MGT and where lipid II-Lys was replaced by 0.01% (v/v) Triton X-100 (Trace **c**). All assays were performed in triplicate and are shown ± standard deviation. **Panel (b)**: Impact of a non-polymerizable donor and a polymerizable acceptor on PBP1B transpeptidation. To transpeptidase assays containing 20 μM of the putative non-polymerizable donor (MurNAc *meso*-DAP pentapeptide or lipid I Lys; Traces **a** and **d** respectively) was added after 2 minutes and 8 minutes, 45.1 nM PBP1B and 20 μM lipid II-*meso*-DAP

tetrapeptide respectively as the polymerizable acceptor. Finally, to confirm assay functionality, assays were supplemented with 60 μM Lipid II-Lys. Additionally, controls were run where MurNAc *meso*-DAP pentapeptide and lipid I-Lys were replaced by water (Trace **b**) or 0.01% (v/v) Triton X-100 (Trace **c**) respectively. Absorbance at 555 nm was monitored throughout. **Panel (c)** Impact of the non-polymerizable donor lipid I-*meso*-DAP and a polymerizable acceptor on PBP1B transpeptidation. Transpeptidase assays contained 20 μM of putative non-polymerizable donor lipid I-*meso*-DAP, 20 μM lipid II-Lys (positive control) or 0.01% (v/v) Triton X-100 as negative control (Traces **a**, **b** and **c** respectively). After 2 minutes and 8 minutes respectively, 9.01 nM PBP1B and 20 μM lipid II-*meso*-DAP tetrapeptide (polymerizable acceptor) were added. **Panel (d)** SDS-PAGE assay of monofunctional transglycosylase (MGT) polymerization of lipid II-Lys. Assays were carried out, electrophoretically fractionated and the resulting polymeric products visualised as described in **S.1.2.7.**

Figure S8: Evaluation of the impact of modification of the donor stem peptide third position residue on transpeptidase activity. To transpeptidase assays containing 20 μM lipid II-Lys donor or analogues thereof where the stem peptide *L*-lysine was replaced by *L*-arginine or 5 hydroxy *L*-lysine, or where the ε-amino group of the lysine was methylated, biotinylated or dansylated, was added 8.49 nM PBP1B after 2 minutes. At 8 minutes assays were supplemented with 20 μM MurNAc *meso*-DAP pentapeptide. Absorbance at 555 nm was monitored throughout. Control assays were run without donor. Left hand panel: Structure of lipid II-Lys and the third position stem peptide lysine substitutions. Right-hand panel, histogram of PBP1B carboxypeptidase (**CP**) or transpeptidase (**TP**) initial rates (shaded purple or red) supported by the different donors. Error bars are standard deviations of triplicate assays.

Figure S9: Impact of donor amidation on PBP1B activity. Panel (a): Structure of amidated lipid II-Lys compared to lipid II-Lys. Left-hand blue structure, lipid II-Lys with the

undecaprenyl pyrophosphoryl (**UPP**) moiety highlighted in magnolia and the hydroxyl that is replaced by NH_2 on amidation of the stem peptide glutamate α-carboxyl in amidated lipid II-Lys highlighted with a gold circle. Right-hand maroon structure, amidated lipid II-Lys with the **UPP** moiety highlighted in magnolia and NH_2 that replaces the hydroxyl of the stem peptide glutamate α-carboxyl of lipid II-Lys highlighted with a gold circle. **Panel (b)**: Assay of the impact of amidation of the lipid donor on PBP1B transpeptidation. *E. coli* PBP1B transpeptidase activity assay (Main Manuscript) with 4.4 nM *E. coli* PBP1B, 20 μM Lipid II-Lys (blue trace **ia**) or 20 μM amidated Lipid II-Lys (maroon trace **iia**) as donors and 20 μM MurNAc *meso*-DAP pentapeptide acceptor with two controls where 0.01% (v/v) Triton X-100 replaced lipid II-Lys (trace **ib**) or amidated Lipid II-Lys (trace **iib**). Absorbance at 555 nm was monitored for two minutes prior to the addition of PBP at **(1)** and for a further 6 minutes at which point **(2)** the acceptor was added to initiate the transpeptidation rate. After 33 minutes **(3)** the [*E. coli* PBP1B] was increased by addition of a further 4.4 nM enzyme to the assays carried out with amidated lipid II-Lys (trace **iia**). **Panels (c** and **d)**: assay of the impact of amidation of the lipid donor on PBP1B transglycosylation. For both panels, PBP1B (4.4 nM) was assayed in the transpeptidase assay in the presence of 20 μM amidated lipid II-lys and 20 μM MurNAc *meso*-DAP pentapeptide. Assays were then fractionated and analysed by negative ion nanospray time of flight mass spectrometry (**S.1.2.3.2.2**). % values (white type in grey box appended to each mass spectrum) correspond to the proportion of 2:1 isopropanol/methanol in the eluant of the Bond Elut CN-E reverse phase columns used to fractionate the amidated lipid II-Lys substrate and undecaprenyl pyrophosphate in these assays. **Panel (c)**: 50 μM moenomycin was added to stop the reaction at the end of the assay. Doubly charged ions corresponding to amidated lipid II-Lys were absent while the transglycosylase product (undecaprenyl pyrophosphate, expected $(m\text{-}H^+)/1 = 925.62$) was observed as the singly charged anion eluting in eluant washes containing 50-80% (v/v)

isopropanol:methanol (2:1) with observed (m-H^+)/1 = 925.63 in all washes. **Panel (d)**: the control reaction where 50 μM moenomycin was added to the assay before PBP1B, to inhibit the transglycosylase activity of this enzyme. Here elution of amidated lipid II-Lys was observed (expected (m-$2H^+$/2) = 936.03; observed (m-$2H^+$/2) for 40, 50, 60, 70 and 80% (v/v) washes = 936.04, 936.03, 936.03, 936.04 and 936.05 respectively). No ion corresponding to undecaprenyl pyrophosphate (expected (m-H^+)/1 = 925.62) was detected in assays conducted in the presence of moenomycin.

Figure S10: Impact of substitution of *L*-alanine for *D*-alanine at the C-terminus of the stem peptide of the Lipid II-Lys transpeptidase donor of PBP1B. Panels (a and **b)**: Assay of the impact of substitution of *L*-alanine for *D*-alanine at the C-terminus of the stem peptide of the Lipid II-Lys on PBP1B transglycosylation. For both panels, 8.62 nM PBP1B transpeptidase activity was assayed with 20 μM lipid II-Lys (*L*-Ala) as prospective donor and 20 μM MurNAc *meso*-DAP pentapeptide acceptor (main paper Methods) and further fractionated and analysed by negative ion nanospray time of flight mass spectrometry (**S.1.2.3.2.2**). % values (white type in grey box appended to each mass spectrum) correspond to the proportion of 2:1 isopropanol/methanol in the eluant of the Bond Elut CN-E columns used to fractionate lipid II-Lys (*L*-Ala) substrate and undecaprenyl pyrophosphate product in these assays. **Panel (a)**: 50 μM moenomycin was added to stop the reaction at the end of the assay. Doubly charged ions corresponding to lipid II-Lys (*L*-Ala) were absent while the transglycosylase product (undecaprenyl pyrophosphate, expected (m-H^+)/1 = 925.62) was observed in eluant washes containing 50, 60, 70, and 80% (v/v) isopropanol:methanol (2:1) with observed (m-H^+)/1 = 925.63 in all washes. **Panel (b)**: 50 μM moenomycin was added to the assay prior to PBP1B, to inhibit its transglycosylase activity. Elution of lipid II-Lys (*L*-Ala) was observed between 40 and 60% (v/v) 2:1 isopropanol/methanol (Expected (m-$2H^+$/2) = 936.52; observed (m-$2H^+$/2) for 40, 50 and 60% (v/v) washes = 936.52, 936.52 and 936.51 respectively). Undecaprenyl pyrophosphate was

undetectable in this instance. **Panel (c):** Continuous assay of PBP1B catalysed release of *L*-alanine. Continuous transpeptidation assays designed to follow *L*-alanine release (main paper Methods) containing either 20 μM lipid II-Lys (*L*-Ala) (trace **c**(**iii**)) or lipid II-Lys (trace **c**(**ii**)) or both lipids (trace **c**(**i**)) were supplemented by 8.49 nM PBP1B after 2 minutes. After a further 8 minutes, assays were supplemented with 20 μM MurNAc *meso*-DAP pentapeptide. Negative control assays were run where lipid II-Lys (*L*-Ala) was replaced by 0.01% (v/v) Triton X-100 (trace **c**(**iv**)). Absorbance at 555 nm was monitored throughout. **Panel (d)**: Discontinuous assay of PBP1B catalysed release of *L*-alanine and *D*-alanine from: **(i) Lipid II-Lys (*L*-Ala)**. Discontinuous transpepetidase assay designed to follow *L*-alanine release (main paper Methods). At time zero, assays contained 20 μM lipid II-Lys (*L*-Ala), 20 μM MurNAc *meso*-DAP pentapeptide and 34.5 nM *E. coli* PBP1B (Trace (**i**)); 20 μM lipid II-Lys (*L*-Ala) and 34.5 nM *E. coli* PBP1B (Trace (**ii**)); 0.01% (v/v) Triton X-100, 20 μM MurNAc *meso*-DAP pentapeptide and 34.5 nM *E. coli* PBP1B (Trace (**iii**)) and 20 μM lipid II-Lys (*L*-Ala) and 20 μM MurNAc *meso*-DAP pentapeptide (Trace (**iv**)). After 60 minutes, assays were stopped with 2.86 mM ampicillin and supplemented (including alanine racemase) as described (main paper Methods). The assays were followed for a further 24 minutes at which point, 4 μM *L*-alanine was added to Trace (**iv**) to confirm assay functionality. **(ii) Lipid II-Lys**. Discontinuous transpepetidase assay to follow *D*-alanine release (main paper Methods). All assays corresponding to Trace (**i**), (**ii**), (**iii**) and (**iv**) in the lipid II-Lys (*L*-Ala) experiment were constituted identically where lipid II-Lys replaced lipid II-Lys (*L*-Ala). After 60 minutes, assays were supplemented with 2.86 mM ampicillin and supplemented as described (main paper Methods) without alanine racemase to detect *D*-alanine release. The brief absorbance change on addition of the coupling enzyme mix in Panel **(d)(i)** is independent of PBP1B or its substrates and is likely contributed by residual peroxide accumulation in the Triton X-

100 in the assay, pyridoxal phosphate, D-amino acid oxidase, FAD and traces of resorufin in the amplex red.

Figure S11: LCMSMS analysis of the structure of the transpeptidation products of PBP1B formed from lipid II-*L*,*L*-DAP and between lipid II-*L*,*L*-$^{\varepsilon}$NAc-DAP and MurNAc *meso*-DAP pentapeptide. **Panel (a)**: the mass spectrum of the fragmentation of the lipid II-*L*,*L*-DAP transpeptidation product of PBP1B. This molecule, detected in a survey chromatogram as its doubly charged anomers (structure equivalent to that in Figure 2a) eluting at 7.94, 7.70 and 7.40 minutes (m+2H+)/2 expected = 966.92, observed = 966.91, 966.92 and 966.91 respectively) was subjected to MSMS fragmentation (**S.1.2.3.2.1**). The fragmentation pattern of the 966.91 m/z species (**Panel (a)**) from the 7.94 minute peak was superimposable over that obtained from equivalent analysis of the 7.70 and 7.40 minute peaks. All fragments that contain transpeptidation crosslinks are denoted by a purple number with a yellow square surround and labelled with a yellow T in a green circle, whereas fragments that do not contain this linkage are denoted by a yellow number with a purple surround. Fragment numbering corresponds to the numbering of fragment structures in Table S3. **Panel (b)**: the mass spectrum of the fragmentation of the transpeptidation product of PBP1B formed from lipid II-*L*,*L*-$^{\varepsilon}$NAc-DAP and MurNAc *meso*-DAP pentapeptide. This molecule, detected in a survey chromatogram as its doubly charged anomers (Figure 4c) eluting at 8.21, 8.02 and 7.86 minutes ((m+2H+)/2 expected = observed = 886.38 for these peaks) was fragmented (**S.1.2.3.2.1**) yielding the fragmentation pattern in **Panel (b)** from the 8.21 minute peak (Figure 4c) which was superimposable over that obtained from the 8.02 and 7.86 minute peaks. Labelling is as in Panel (a). Fragment numbering corresponds to the numbering of fragment structures in Table S7.

Figure S12: Variation of kinetics of acceptor utilization by PBP1B. All assays were carried out with 20 μM lipid II-Lys donor. Acceptor and *E. coli* PBP1B concentrations are recorded in Table 1. All data were fitted using GraphPad Prizm vers. 8 to Equation 1 in the main manuscript. All error bars are ± standard deviations of triplicate determinations. Graphs show dependence of transpeptidation initial rate (v_o) on [lipid I-*meso*-DAP], [lipid II-*meso*-DAP tetrapeptide], [MurNAc *meso*-DAP pentapeptide], [MurNAc *meso*-DAP pentapeptide-NH_2], [MurNAc *meso*-DAP tetrapeptide], [MurNAc *meso*-DAP tetrapeptide-NH_2], [MurNAc *meso*-DAP tripeptide], [MurNAc *meso*-DAP tripeptide-NH_2], [*D*-Lactate] and [*L*-Alanine] (**Panels (a)**-**(j)** respectively).

Figure S13: Theoretical relationships of v_o *vs* MurNAc *meso*-DAP tripeptide concentration at varying lipid II Lys described by equations 3 and S2-S4 fitted to experimental data. All assays were carried out with the indicated substrate concentrations. Error bars are ± standard deviations of triplicate determinations. Data points in each panel were fitted using MATLAB 2017a by non-linear regression to equations 3, S2, S3 and S4 which describe relationships obeying random rapid equilibrium, ordered rapid equilibrium (lipid II-Lys first), ordered rapid equilibrium (MurNAc *meso*-DAP tripeptide first) and Ping Pong mechanisms. The graph representing the random rapid equilibrium fit (Equation 3) in this figure is the same as Figure 5h in the main text.

Table S1

Observed and expected m/z values on mass spectrometric analysis of UDP precursors of PBP1B substrates and inhibitors

UDP MurNAc peptide precursor	m-1/1		m-2/2		m-3/3	
	Expected	Observed	Expected	Observed	Expected	Observed
UDP MurNAc *L*-Ala-*D*-γ Glu-*meso*-DAP-*D*-Ala-*D*-Ala	1192.33	1192.35	595.66	595.67	396.77	396.78
UDP MurNAc *L*-Ala-*D*-γ Glu-*L*,*L*-DAP-*D*-Ala-*D*-Ala	1192.33	-	595.66	595.67	396.77	-
UDP MurNAc *L*-Ala-*D*-γ Glu-*L*-Lysyl-*D*-Ala-*D*-Ala	1148.34	1148.34	573.66	573.67	382.10	382.12
UDP MurNAc *L*-Ala-*D*-γ Glu-*L*-Lysyl-*D*-Ala-*L*-Ala	1148.34	1148.34	573.66	573.69	382.10	382.12
UDP MurNAc *L*-Ala-*D*-γ Glu-*meso*-DAP-*D*-Ala	1121.29	1121.22	560.14	560.10	373.09	-
UDP MurNAc *L*-Ala-*D*-γ Glu-*L*,*L*-DAP-*D*-Ala	1121.29	1121.29	560.14	560.14	373.09	-
UDP MurNAc *L*-Ala-*D*-^{i}Gln-Lysyl-*D*-Ala-*D*-Ala	1147.36	1147.35	573.18	573.17	381.78	381.78
UDP MurNAc *L*-Ala-*D*-^{i}Gln-*meso*-DAP-*D*-Ala-*D*-Ala	1191.35	1191.35	595.17	595.17	396.44	-

UDP MurNAc *L*-Ala-*D*-γ Glu-L-(ᵋdansyl)-Lysyl-*D*-Ala-*D*-Ala	1381.39	1381.40	690.19	690.16	459.79	-
UDP MurNAc *L*-Ala-*D*-γ Glu-L-(ᵋbiotinyl)-Lysyl-*D*-Ala-*D*-Ala	1374.42	1374.42	686.71	686.71	457.46	457.47
UDP MurNAc *L*-Ala-*D*-γ Glu-*L*-Arginyl-*D*-Ala-*D*-Ala	1176.34	1176.24	587.67	587.67	391.44	391.44
UDP MurNAc *L*-Ala-*D*-γ Glu-L-(ᵋmethyl)-Lysyl-*D*-Ala-*D*-Ala	1162.35	1162.24	580.67	580.65	386.78	386.78
UDP MurNAc *L*-Ala-*D*-γ Glu-L-5-Hydroxy-Lysyl-*D*-Ala-*D*-Ala	1164.33	1164.21	581.66	581.64	387.44	387.44
CH2-UDP MurNAc *L*-Ala-*D*-γ Glu-L-Lysyl-*D*-Ala-*D*-Ala	1146.37	1146.39	572.68	572.68	381.45	381.46
UDP MurNAc *L*-Ala-*D*-γ Glu-*meso*-DAP	1050.26	1050.26	524.62	524.63	349.41	349.42
UDP MurNAc *L*-Ala-*D*-ⁱGln-*meso*-DAP-*D*-Ala	1120.31	1120.32	559.65	559.66	372.77	372.77
UDP MurNAc *L*-Ala-*D*-ⁱGln-*meso*-DAP	1049.28	1049.27	524.13	524.13	349.08	-
UDP MurNAc *L*-Ala-*D*-γ Glu-*L*,*L*-(ᵋN-acetyl*)*-DAP-*D*-Ala-*D*-Ala	1234.34	1234.35	616.67	616.68	410.78	410.78
UDP MurNAc *L*-Ala-*D*-γ Glu-*meso*-(ᵋN-acetyl*)*-DAP-*D*-Ala-*D*-Ala	1234.34	1234.35	616.67	616.67	410.78	410.78
UDP MurNAc *L*-Ala-*D*-γ Glu	878.18	878.20	438.58	438.59	292.06	292.06

Table S2

Observed and expected m/z values on mass spectrometric analysis of PBP1B donors and acceptors and analogues thereof

Substrate	PBP Function Tested	m-1/1		m-2/2		m-3/3	
		Expected	Observed	Expected	Observed	Expected	Observed
Lipid II-*meso*-DAP	Donor/Acceptor	1918.04	1918.04	958.51	958.51	638.67	638.67
Lipid II-*L*,*L*-DAP	Donor	1918.04	1918.04	958.51	958.52	638.67	638.67
Lipid II-*L*,*L*-$^{\varepsilon}$NAc.DAP	Donor	1960.05	1960.06	979.52	979.53	652.68	652.68
Lipid II-*meso*-$^{\varepsilon}$NAc.DAP	Donor	1960.05	1960.05	979.52	979.52	652.68	652.68
Lipid II-Lys	Donor	1874.05	1874.06	936.52	936.53	624.01	624.02
Amidated Lipid II-Lys	Donor	1873.07	1873.07	936.03	936.03	623.68	-
Lipid II $^{\varepsilon}$N-dansyl-Lys	Donor	2107.10	2107.10	1053.05	1053.05	701.69	-
Lipid II-$^{\varepsilon}$N-biotinyl-Lys	Donor	2100.13	-	1049.56	1049.58	699.37	699.39
Lipid II-Arg	Donor	1902.06	1902.06	950.53	950.53	633.35	633.35
Lipid II-$^{\varepsilon}$N-methyl-Lys	Donor	1888.07	1888.07	943.53	943.53	628.68	628.68
Lipid II-5-hydroxy-Lys	Donor	1890.05	1890.05	944.52	944.52	629.34	629.34
Lipid II-*meso*-DAP tetrapeptide	Acceptor	1847.01	1846.99	922.99	922.99	614.99	615.00

Lipid II-*L*,*L*-DAP tetrapeptide	Acceptor	1847.01	-	922.99	922.99	614.99	-
Lipid I-*meso*-DAP	Acceptor	1714.96	1714.95	856.98	856.98	570.98	570.99
Lipid I-Lys	Donor or Acceptor	1670.97	1670.97	835.00	834.98	556.32	556.32
MurNAc *meso*-DAP tripeptide	Acceptor	664.27	664.27	331.63	331.63	220.75	-
MurNAc *meso*-DAP tetrapeptide	Acceptor	735.30	735.31	367.15	367.15	244.43	-
MurNAc *meso*-DAP pentapeptide	Acceptor	806.34	806.34	402.67	402.67	268.11	-
MurNAc *meso*-DAP tripeptide-NH_2	Acceptor	663.28	663.28	331.14	331.14	220.42	-
MurNAc *meso*-DAP tetrapeptide-NH_2	Acceptor	734.32	734.32	366.66	366.67	244.10	-
MurNAc *meso*-DAP pentapeptide-NH_2	Acceptor	805.36	805.36	402.18	402.17	267.78	-
Lipid II-Lys (*L*-Ala)	Donor or inhibitor	1874.05	1874.06	936.52	936.53	624.01	624.02
Methylene Lipid II-Lys	Donor or inhibitor	1872.07	1872.07	935.53	935.54	623.35	623.36
MurNAc *L*-Ala-γ-*D*-Glu	Inhibitor	492.18	492.18	245.59	-	163.39	-

Table S3

Identification of MSMS collision-induced fragment ions of PBP1B transpeptidation products derived from lipid II-*meso*-DAP and lipid II-*L,L*-DAP

Species	Observed (m+1)/1		Putative structure	Expected (m+1)/1
	Lipid II-*meso*-DAP	Lipid II-*L,L*-DAP		
1	1508.66	1508.63	MurNAc.A.E.DAP.A | MurNAc.A.E.DAP.A.A -H_2O	1508.65
2	1490.64	1490.62	MurNAc.A.E.DAP.A | MurNAc.A.E.DAP.A.A -$2H_2O$	1490.64
3	1401.59	1401.60	MurNAc.A.E.DAP.A | MurNAc.A.E.DAP.A -$2H_2O$	1401.59
4	1305.57	1305.58	MurNAc.A.E.DAP.A | Lactyl.A.E.DAP.A.A -H_2O or Lactyl.A.E.DAP.A | MurNAc.A.E.DAP.A.A -H_2O	1305.57
5	1287.55	1287.55	MurNAc.A.E.DAP.A | Lactyl.A.E.DAP.A.A -$2H_2O$ or Lactyl.A.E.DAP.A | MurNAc.A.E.DAP.A.A -$2H_2O$	1287.56
6	1216.53	1216.54	MurNAc.A.E.DAP.A | Lactyl.A.E.DAP.A -H_2O or Lactyl.A.E.DAP.A | MurNac.A.E.DAP.A -H_2O	1216.52
7	1162.51	1162.51	E.DAP.A | MurNAc.A.E.DAP.A.A -H_2O or MurNAc.A.E.DAP.A | E.DAP.A.A -H_2O	1162.51
8	1145.50	1145.49	MurNAc.A.E.DAP.A | Lactyl.A.E.DAP or Lactyl.A.E.DAP.A | MurNAc.A.E.DAP	1145.49
9	1120.50	1120.51	Lactyl.A.E.DAP.A | Lactyl.A.E.DAP.A.A	1120.50
10	1102.52	1102.49	Lactyl.A.E.DAP.A | Lactyl.A.E.DAP.A.A -H_2O	1102.49
11	1073.46	1073.46	MurNAc.A.E.DAP.A | A.E.DAP -H_2O or A.E.DAP.A | MurNAc.A.E.DAP -H_2O	1073.46
12	1033.47	1033.47	DAP.A | MurNAc.A.E.DAP.A.A -H_2O or MurNAc.A.E.DAP.A | DAP.A.A -H_2O	1033.47
13	977.44	977.44	Lactyl.A.E.DAP.A | E.DAP.A.A or E.DAP.A | Lactyl.A.E.DAP.A.A	977.44
14	960.42	960.42	Lactyl.A.E.DAP.A | E.DAP.A.A -H_2O or E.DAP.A | Lactyl.A.E.DAP.A.A -H_2O	960.44

15	888.40	888.40	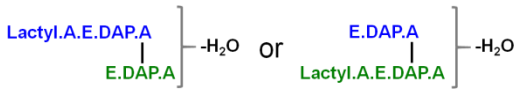	888.40
16	861.39	861.39		861.38
17	848.40	848.40	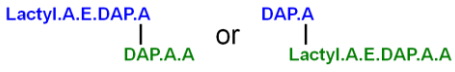	848.40
18	817.36	817.36	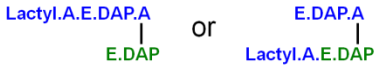	817.36
19	799.36	799.35	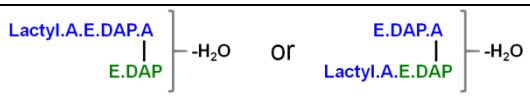	799.35
20	790.35	790.36	MurNAc.A.E.DAP.A.A -H2O	790.35
21	772.34	772.33	MurNAc.A.E.DAP.A.A -2H2O	772.34
22	705.34	705.34	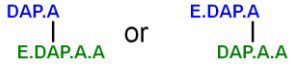	705.34
23	701.30	701.30	MurNAc.A.E.DAP.A -H2O	701.30
24	676.32	676.32		676.32
25	630.26	630.27	MurNAc.A.E.DAP -H2O	630.26
26	605.28	605.28	Lactyl.A.E.DAP.A.A	605.28
27	587.27	587.27		587.27
28	576.29	576.30	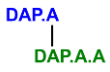	576.30
29	545.26	545.26	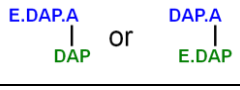	545.26
30	533.26	533.26		533.26
31	516.23	516.23		516.23
32	498.23	498.22	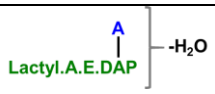	498.22
33	462.22	462.23	E.DAP.A.A	462.22
34	445.19	445.20	Lactyl.A.E.DAP	445.19
35	444.21	444.20	A.E.DAP.A	444.21

36	416.21	416.21		416.22
37	404.21	404.21		404.22
38	373.17	373.17	A.E.DAP or E.DAP. A	373.17
39	333.15	333.18	DAP.A.A	333.17
40	329.17	329.13	MurNAc.A $-H_2O$	329.13
41	315.17	315.17		315.17
42	302.14	302.13	E.DAP	302.14
43	244.14	244.13	DAP. A	244.13
44	204.09	204.08	GlcNAc $-H_2O$	204.09

Table S4

Identification of MSMS collision-induced fragment ions of PBP1B carboxypeptidation products derived from lipid II-*meso*-DAP and lipid II-*L*,*L*-DAP

Species	Observed (m+1)/1		Putative structure	Expected (m+1)/1
	Lipid II-*L*,*L*-DAP	Lipid II-*meso*-DAP		
1	ND	940.42	GlcNAc.MurNAc.A.E.DAP.A	940.40
2	922.36	922.39	GlcNAc.MurNAc.A.E.DAP.A – H_2O	922.39
3	ND	737.33	MurNAc.A.E.DAP.A	737.32
4	719.30	719.31	MurNAc.A.E.DAP.A – H_2O	719.31
5	701.32	701.29	MurNAc.A.E.DAP.A – $2H_2O$	701.30
6	ND	630.26	MurNAc.A.E.DAP – H_2O	620.26
7	612.25	612.26	MurNAc.A.E.DAP.A – $2H_2O$	612.25
8	534.24	534.24	Lactyl.A.E.DAP.A	534.24
9	516.21	516.23	Lactyl.A.E.DAP.A – H_2O	516.23
10	462.26	462.22	A.E.DAP.A	462.22
11	445.19	445.19	Lactyl.A.E.DAP	445.19
12	391.18	391.18	E.DAP.A	391.18
13	373.17	373.17	A.E.DAP	373.17
14	302.13	302.14	E.DAP	302.13
15	262.14	262.14	DAP.A	262.14
16	204.10	204.09	GlcNAc – H_2O	204.09
17	201.09	201.11	A.E	201.09

Table S5

MSMS collision-induced fragment ions of PBP1B transpeptidation products derived from lipid II-Lys and MurNAc *meso*-DAP pentapeptide

Species	Observed (m+1)/1	Putative structure	Expected (m+1)/1
1	1464.66	GlcNAc.MurNAc.A.E.K.A Lactyl.A.E.DAP.A.A -H_2O or MurNAc.A.E.K.A MurNAc.A.E.DAP.A.A -H_2O	1464.66
2	1446.64	GlcNAc.MurNAc.A.E.K.A Lactyl.A.E.DAP.A.A -$2H_2O$ or MurNAc.A.E.K.A MurNAc.A.E.DAP.A.A -$2H_2O$	1446.65
3	1261.58	MurNAc.A.E.K.A Lactyl.A.E.DAP.A.A	1261.58
4	1243.56	MurNAc.A.E.K.A Lactyl.A.E.DAP.A.A -H_2O	1243.57
5	1172.53	Lactyl.A.E.K.A MurNAc.A.E.DAP.A or MurNAc.A.E.K.A Lactyl.A.E.DAP.A	1172.53
6	1118.52	A.E.K.A MurNAc.A.E.DAP.A or MurNAc.A.E.K.A A.E.DAP.A	1118.52
7	1101.50	Lactyl.A.E.K.A Lactyl.A.E.DAP -H_2O	1101.49
8	1100.52	A.E.K.A MurNAc.A.E.DAP.A -H_2O or MurNAc.A.E.K.A A.E.DAP.A -H_2O	1100.51
9	1076.51	Lactyl.A.E.K.A Lactyl.A.E.DAP.A.A	1076.51
10	1058.50	Lactyl.A.E.K.A Lactyl.A.E.DAP.A.A -H_2O	1058.50
11	989.48	MurNAc.A.E.K.A DAP.A.A -H_2O or K.A MurNAc.A.E.DAP.A.A -H_2O	989.48
12	987.48	Lactyl.A.E.K.A Lactyl.A.E.DAP.A	987.46
13	933.45	Lactyl.A.E.K.A DAP.A.A or K.A Lactyl.A.E.DAP.A.A	933.45
14	916.44	Lactyl.A.E.K.A Lactyl.A.E.DAP	916.43
15	915.44	Lactyl.A.E.K.A E.DAP.A.A -H_2O or E.K.A Lactyl.A.E.DAP.A.A -H_2O	915.44

16	898.42	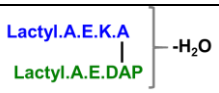	898.42
17	880.40	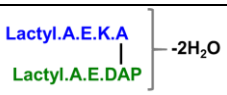	880.41
18	861.39		861.39
19	844.41	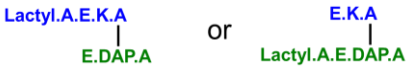	844.41
20	826.39	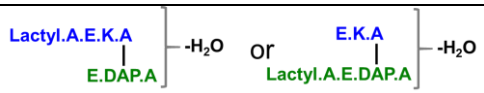	826.40
21	804.41	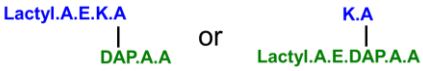	804.41
22	786.40	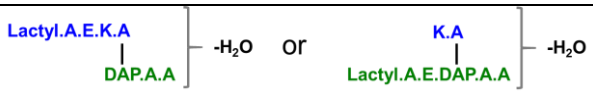	786.40
23	773.37	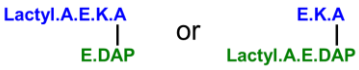	773.39
24	772.37	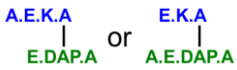	772.38
25	755.36	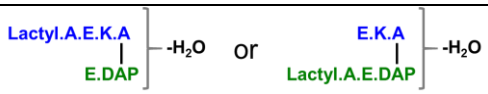	755.36
26	715.36	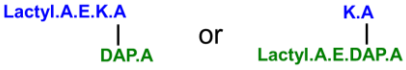	715.36
27	701.29	MurNAc.A.E.DAP.A	701.30
28	676.32		676.32
29	661.35	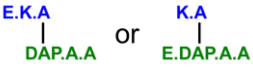	661.35
30	657.31	MurNAc.A.E.K.A -H2O	657.31
31	644.33	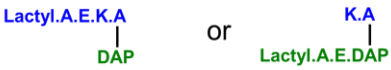	644.33
32	643.33	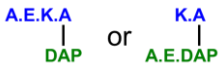	643.34
33	639.30	MurNAc.A.E.K.A -2H2O	639.30
34	630.31		630.31
35	587.27	Lactyl.A.E.DAP.A.A-H2O	587.28

36	572.30	E.K.A | DAP.A or K.A | E.DAP.A	572.30
37	532.31	K.A | DAP.A.A	532.29
38	516.23	Lactyl.A.E.DAP.A or A | Lactyl.A.E.DAP	516.23
39	501.27	K.A | E.DAP or E.K.A | DAP	501.27
40	498.22	Lactyl.A.E.DAP.A $-H_2O$ or A | Lactyl.A.E.DAP $-H_2O$	498.22
41	472.24	Lactyl.A.E.K.A	472.24
42	462.22	E.DAP.A.A	462.22
43	454.23	Lactyl.A.E.K.A $-H_2O$	454.23
44	444.21	A.E.DAP.A	444.21
45	443.26	K.A | DAP.A	443.26
46	427.18	Lactyl.A.E.DAP	427.18
47	404.21	A | DAP.A.A	404.22
48	401.21	Lactyl.A.E.K	401.21
49	373.17	A.E.DAP or A | E.DAP or E.DAP.A	373.17
50	372.22	K.A | DAP	372.23
51	333.17	DAP.A.A	333.18
52	329.18	E.K.A or A.E.K	329.18
53	315.17	A | DAP.A	315.17
54	302.13	E.DAP	302.13
55	258.15	E.K	258.14
56	244.13	DAP.A or A | DAP	244.13
57	204.09	GlcNAc $-H_2O$	204.09

Table S6

Identification of MSMS collision-induced fragment ions of PBP1B carboxypeptidation products derived from lipid II-Lys

Species	Observed (m+1)/1	Putative structure	Expected (m+1)/1
1	896.43	GlcNAc.MurNAc.A.E.K.A	896.41
2	878.40	GlcNAc.MurNAc.A.E.K.A – H_2O	878.40
3	693.33	MurNAc.A.E.K.A	693.33
4	675.32	MurNAc.A.E.K.A – H_2O	675.32
5	657.30	MurNAc.A.E.K.A – $2H_2O$	657.31
6	586.27	MurNAc.A.E.K – H_2O	586.27
7	490.25	Lactyl.A.E.K.A	490.25
8	472.24	Lactyl.A.E.K.A – H_2O	472.24
9	407.19	GlcNAc.GlcNAc	407.17
10	401.20	Lactyl.A.E.K	401.20
11	383.19	Lactyl.A.E.K – H_2O	383.19
12	365.18	GlcNAc.GlcNAc – H_2O – CH_3=O	365.16
13	347.19	E.K.A	347.19
14	329.19	A.E.K	329.18
15	258.15	E.K	258.15
16	240.14	MurNAc – $2H_2O$	240.09
17	218.15	K.A	218.15
18	204.09	GlcNAc – H_2O	204.09
19	201.08	A.E	201.09

Table S7

MSMS collision-induced fragment ions of PBP1B transpeptidation products derived from lipid II-*L*,*L*-$^{\varepsilon}$NAc.DAP and MurNAc *meso*-DAP pentapeptide

Species	Observed (m+1)/1	Putative structure	Expected (m+1)/1
1	1204.51	E.^{Ac}LL-DAP.A | MurNAc.A.E.DAP.A.A -H_2O or MurNAc.A.E.^{Ac}LL-DAP.A | E.DAP.A.A -H_2O	1204.52
2	1075.47	MurNAc.A.E.^{Ac}LL-DAP.A | DAP.A.A -H_2O or ^{Ac}LL-DAP.A | MurNAc.A. E.DAP.A.A -H_2O	1075.50
3	1044.45	E.^{Ac}LL-DAP.A | MurNAc.A.E.DAP -H_2O or MurNAc.A.E.^{Ac}LL-DAP.A | E.DAP -H_2O	1044.37
4	1019.45	E.^{Ac}LL-DAP.A | Lactyl.A.E.DAP.A.A or Lactyl.A.E.^{Ac}LL-DAP.A | E.DAP.A.A	1019.45
5	930.41	E.^{Ac}LL-DAP.A | Lactyl.A.E.DAP.A or Lactyl.A.E.^{Ac}LL-DAP.A | E.DAP.A	930.41
6	890.41	^{Ac}LL-DAP.A | Lactyl.A.E.DAP.A.A or Lactyl.A.E.^{Ac}LL-DAP.A | DAP.A.A	890.41
7	859.37	E.^{Ac}LL-DAP.A | Lactyl.A.E.DAP or Lactyl.A.E.^{Ac}LL-DAP.A | E.DAP	859.37
8	841.36	E.^{Ac}LL-DAP.A | Lactyl.A.E.DAP -H_2O or Lactyl.A.E.^{Ac}LL-DAP.A | E.DAP -H_2O	841.35
9	790.35	MurNAc.A.E.DAP.A.A -H_2O	790.35
10	787.36	A.E.^{Ac}LL-DAP.A | A.E.DAP	787.35
11	772.33	MurNAc.A.E.DAP.A.A -$2H_2O$	772.34
12	747.36	E.^{Ac}LL-DAP.A | DAP.A.A or ^{Ac}LL-DAP.A | E.DAP.A.A	747.35
13	743.31	MurNAc.A.E.^{Ac}LL-DAP.A-H_2O	743.31
14	729.34	^{Ac}LL-DAP.A | Lactyl.A.E.DAP -H_2O or Lactyl.A.E.^{Ac}LL-DAP.A | DAP -H_2O	729.32
15	716.31	E.^{Ac}LL-DAP.A | E.DAP	716.31

16	701.31	MurNAc.A.E.DAP.A -H_2O	701.30
17	676.32		676.32
18	658.30		658.31
19	630.27	MurNAc.A.E.DAP	630.26
20	618.31	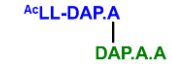	618.31
21	605.27	Lactyl.A.E.DAP.A.A	605.28
22	587.27	Lactyl.A.E.DAP.A.A -H_2O	587.27
23	558.24	Lactyl.A.E.^{Ac}LL-DAP.A	558.24
24	540.22	Lactyl.A.E.^{Ac}LL-DAP.A -H_2O	540.23
25	516.22	Lactyl.A.E.DAP.A or 	516.23
26	498.22	Lactyl.A.E.DAP.A -H_2O or 	498.22
27	487.20	Lactyl.A.E.^{Ac}LL-DAP	487.20
28	469.20	Lactyl.A.E.^{Ac}LL-DAP -H_2O	469.19
29	445.20	Lactyl.A.E.DAP	445.19
30	444.21	 or E.DAP.A	444.21
31	427.18	Lactyl.A.E.DAP -H_2O	427.18
32	415.18	A.E.^{Ac}LL-DAP or E.^{Ac}LL-DAP. A	415.18
33	404.22		404.21
34	373.17	A.E.DAP or  or E.DAP.A	373.17
35	344.15	E.^{Ac}LL-DAP	344.15
36	333.18	DAP.A.A	333.17
37	329.14	MurNAc.A -H_2O	329.14

38	315.16	A | DAP.A	315.17
39	302.13	E.DAP	302.13
40	273.11	Lactyl.A.E	273.11
41	244.13	DAP.A	244.13
42	204.09	GlcNAc -H_2O	204.09

Table S8

Fitted values of kinetic constants and goodness-of-fit measures across the four different equations describing rapid equilibrium random, ordered and Ping Pong Mechanisms

Equation:	3	S2	S3	S4
α	0.13 ± 0.09			
K_{LII} (μM)	25 ± 6	41 ± 6	4×10^{-3} ± 1	23 ± 3
K_{M3P} (μM)	130 ± 80	12 ± 2	1×10^{5} ± 3×10^{7}	55 ± 7
$\underline{V}_{max}$ (min^{-1})	84 ± 5	75 ± 2	58 ± 2	140 ± 10
Number of parameters	4	3	3	3
Sum of squared errors	2409.85	2458.93	4537.21	4021.19
R^2	0.9419	0.9407	0.8906	0.9030
Adjusted r^2	0.9409	0.9400	0.8893	0.9019
Root mean squared error	3.7323	3.7592	5.1065	4.8073

Figure S1

Nanospray Time of flight analysis of lipid II donors and analogues thereof modified at the second, third and fifth position of the pentapeptide stem

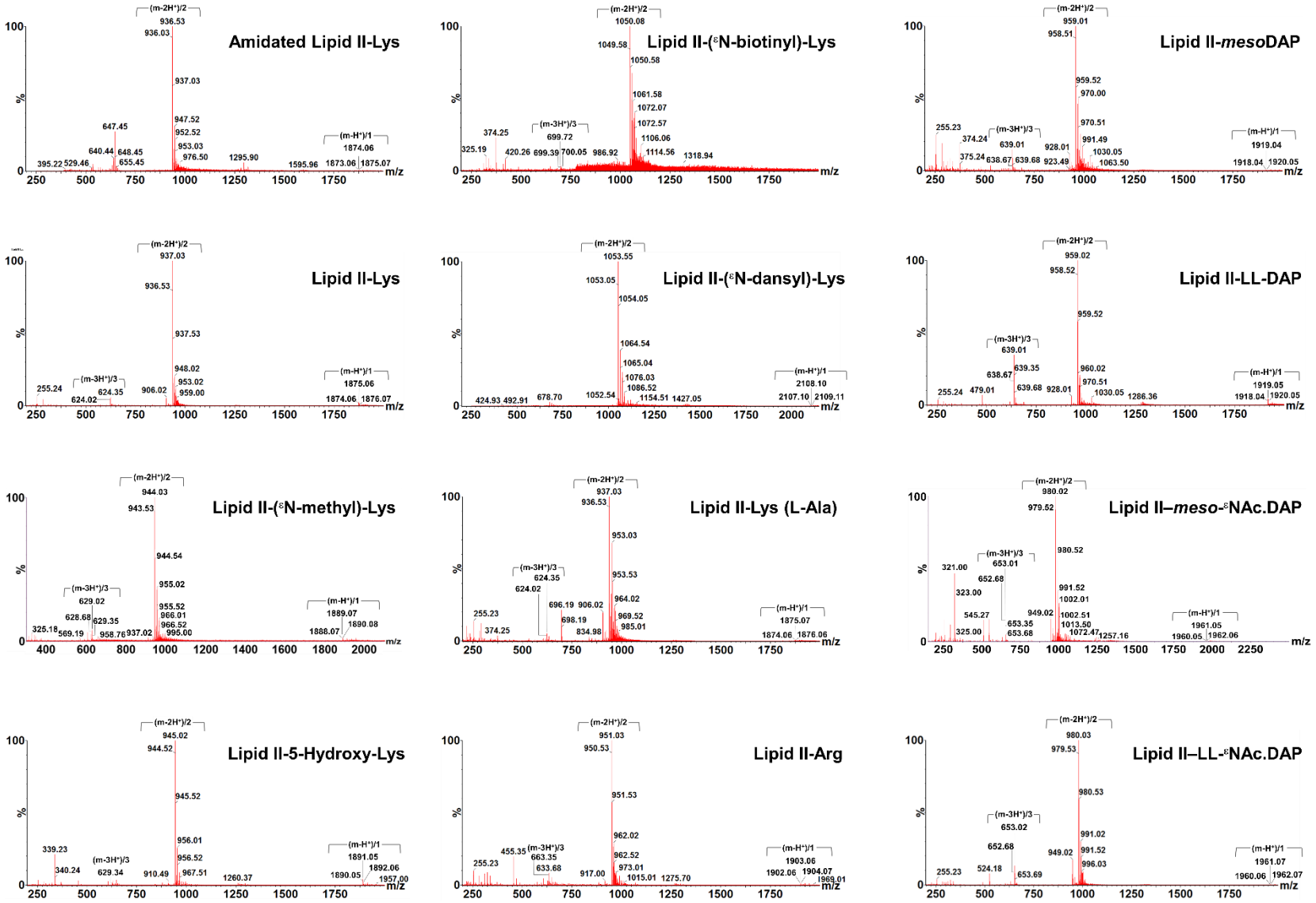

Figure S2

Nanospray Time of flight analysis of inhibitors, acceptors and analogues thereof of *E. coli* PBP1B

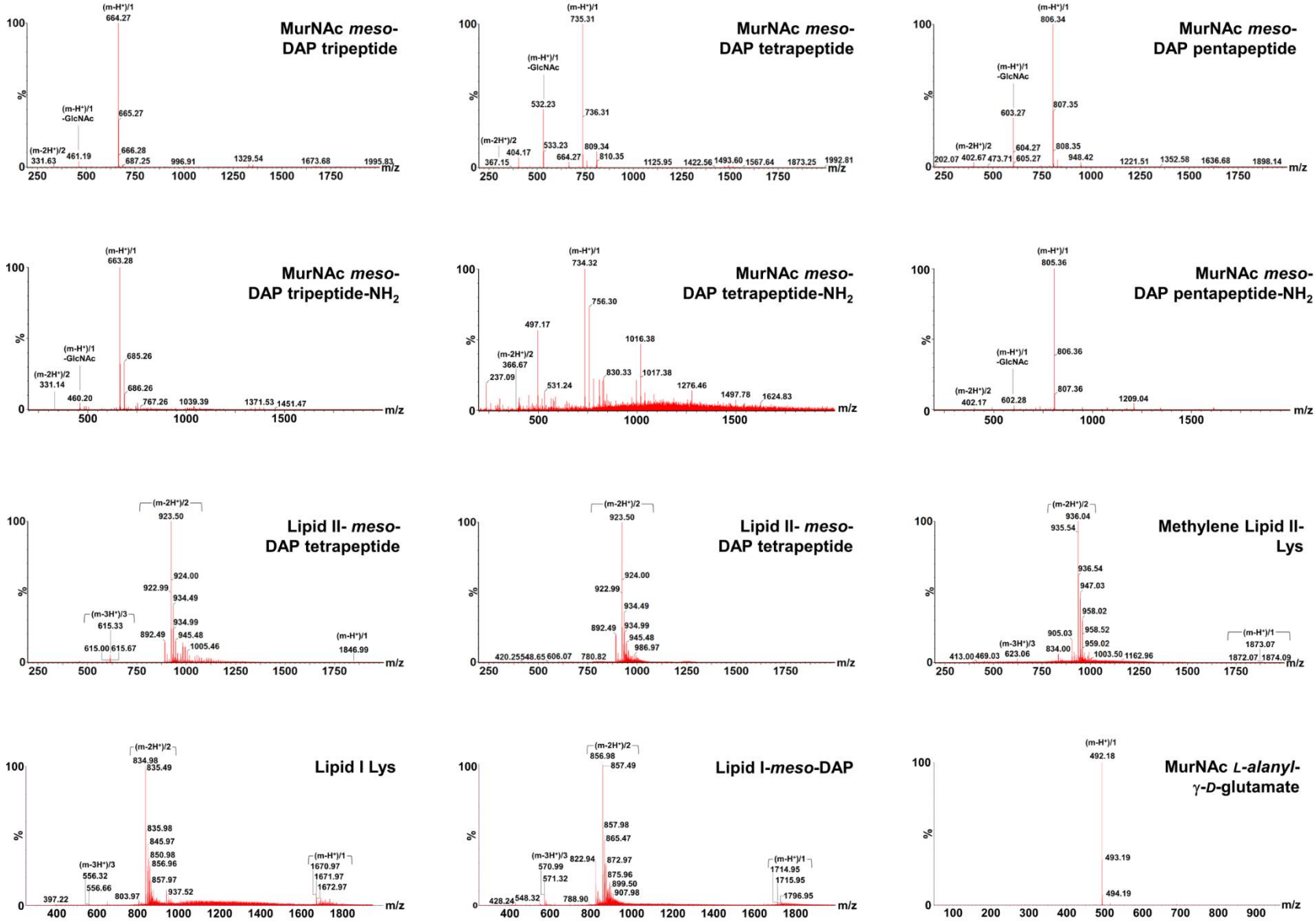

Figure S3

LCMS and LCMSMS of the PBP1B *D,D*-carboxypeptidation product derived from lipid II-*meso*-DAP and lipid II-*L,L*-DAP

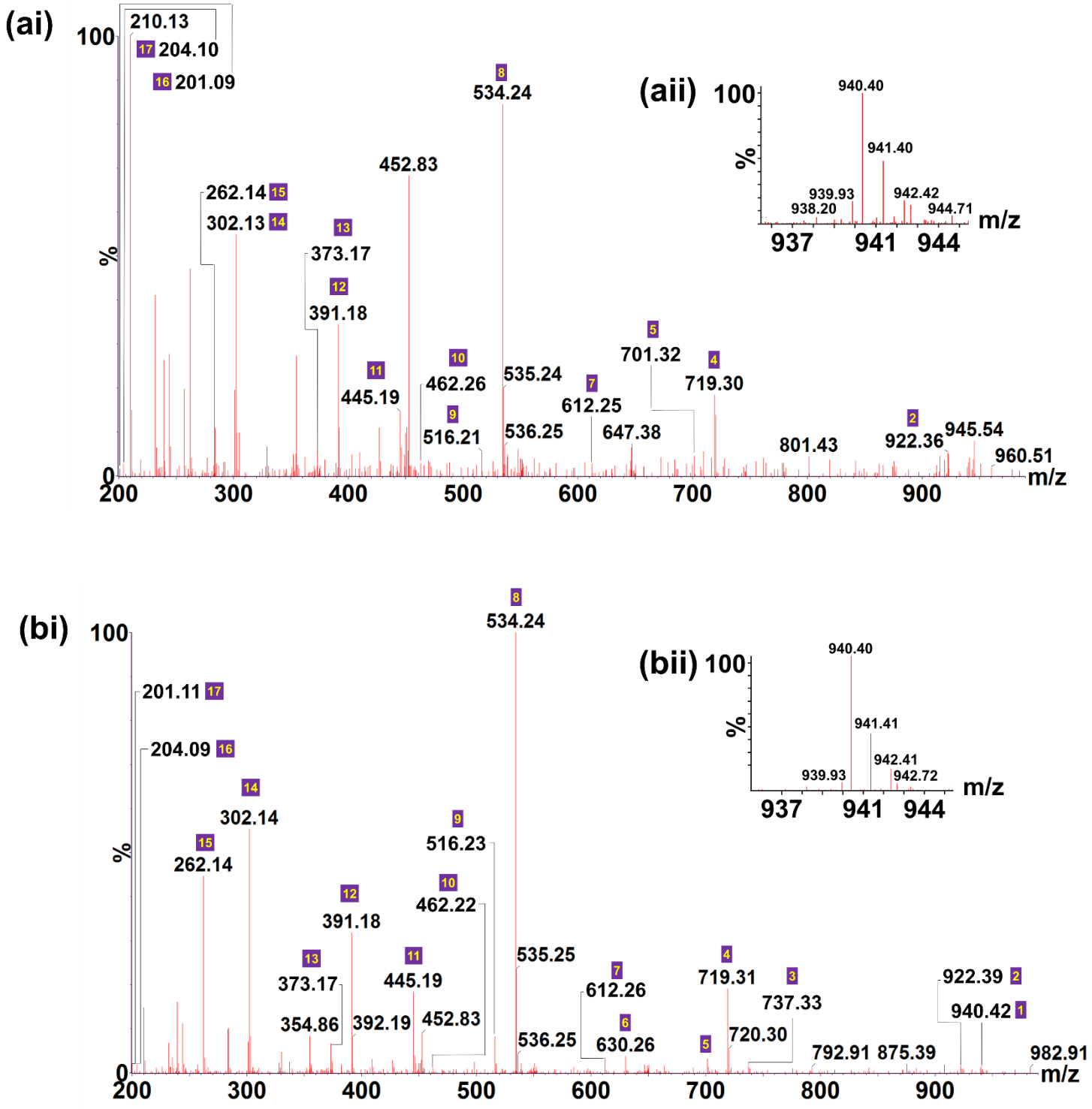

Figure S4

LCMS and LCMSMS of the product of transpeptidation between Lipid II-Lys and MurNAc *meso*-DAP pentapeptide

(a)

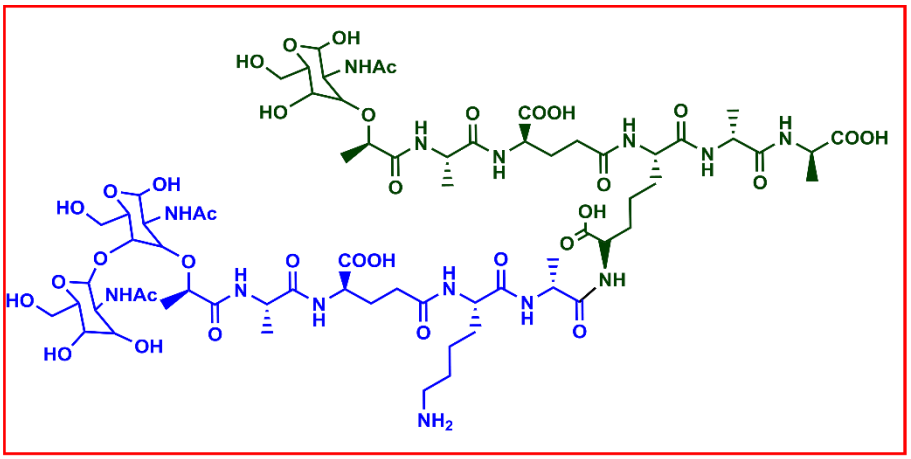

(b)

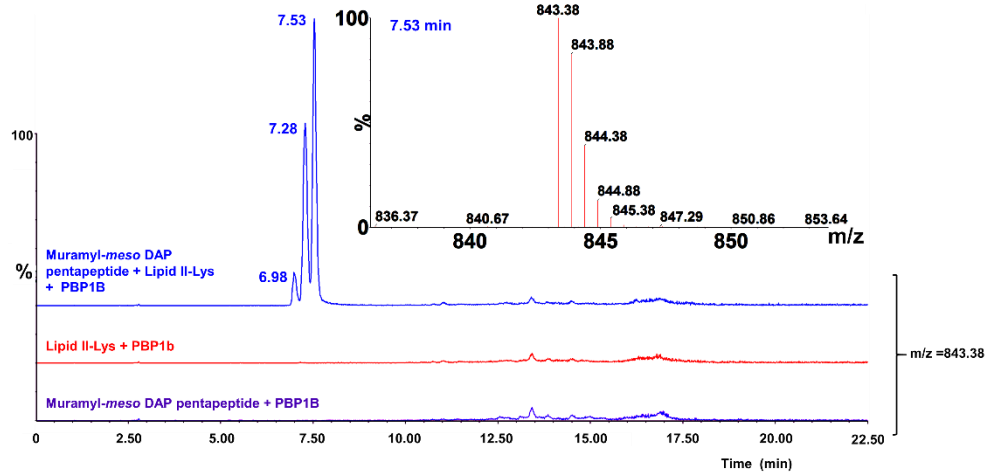

(c)

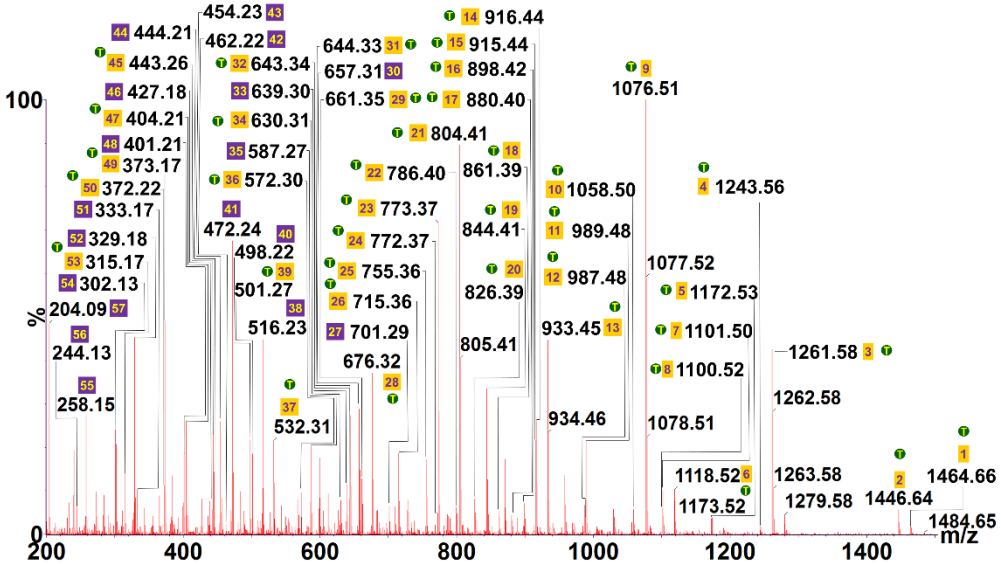

Figure S5

LCMS analysis of the impact of transpeptidation between Lipid II-Lys and MurNAc *meso*-DAP pentapeptide on the residual *D*,*D*-carboxypeptidase activity of PBP1B

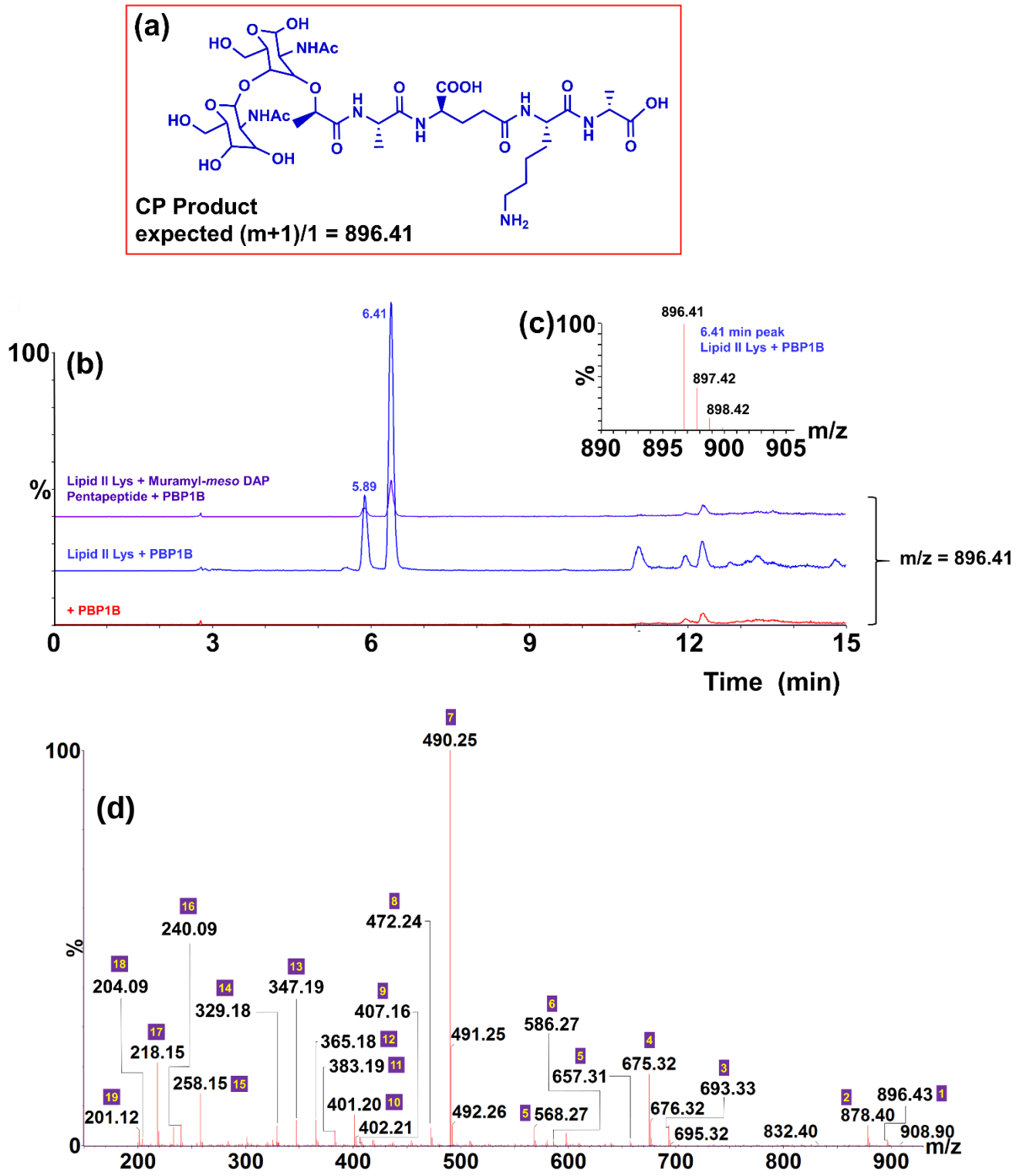

Figure S6

Transglycosylase activity of PBP1B and inhibition of transpeptidase activity by a non-polymerizable analogue of lipid II-Lys and hen egg white lysozyme

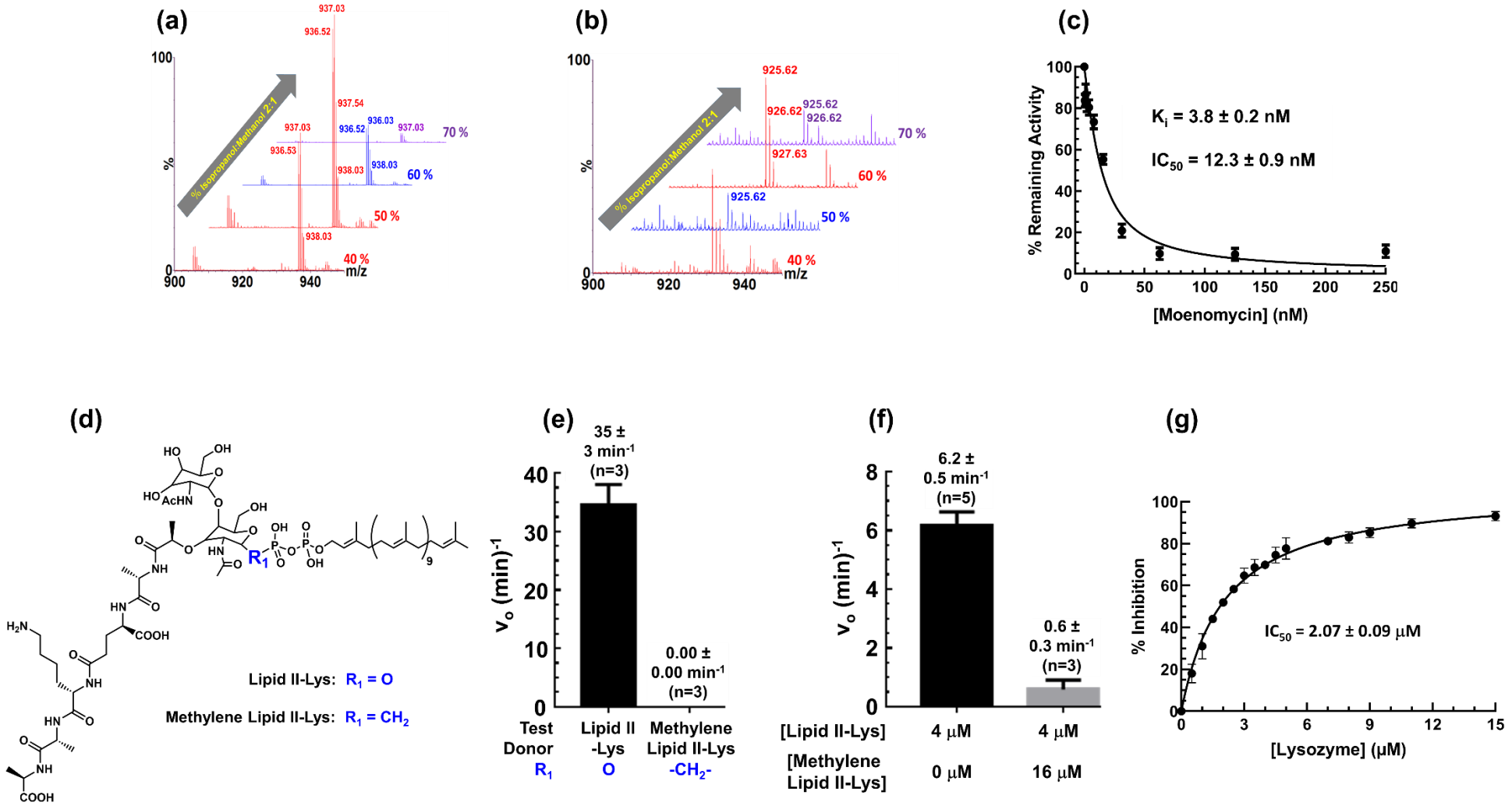

Figure S7

Transpeptidase activity of *E. coli* PBP1B with polymerized and unpolymerizable donors and acceptors

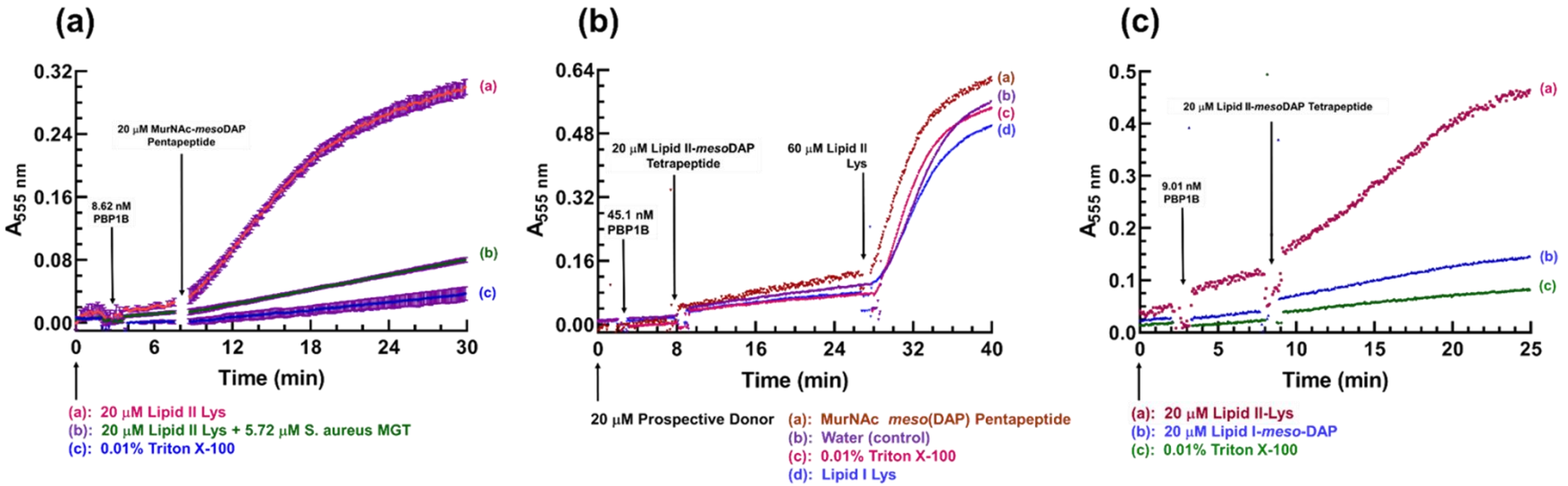

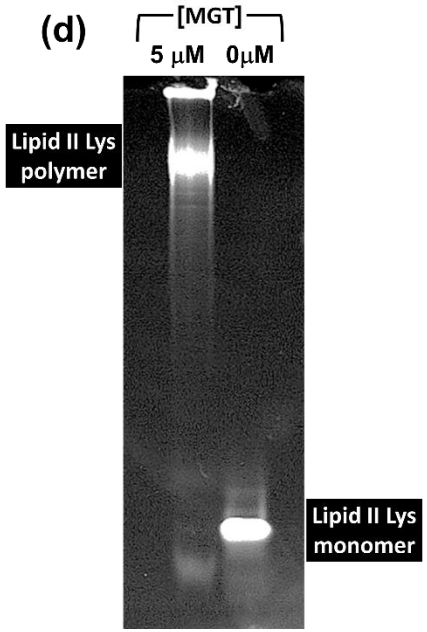

Figure S8

Evaluation of the impact of modification of the donor stem peptide third position residue on transpeptidase activity

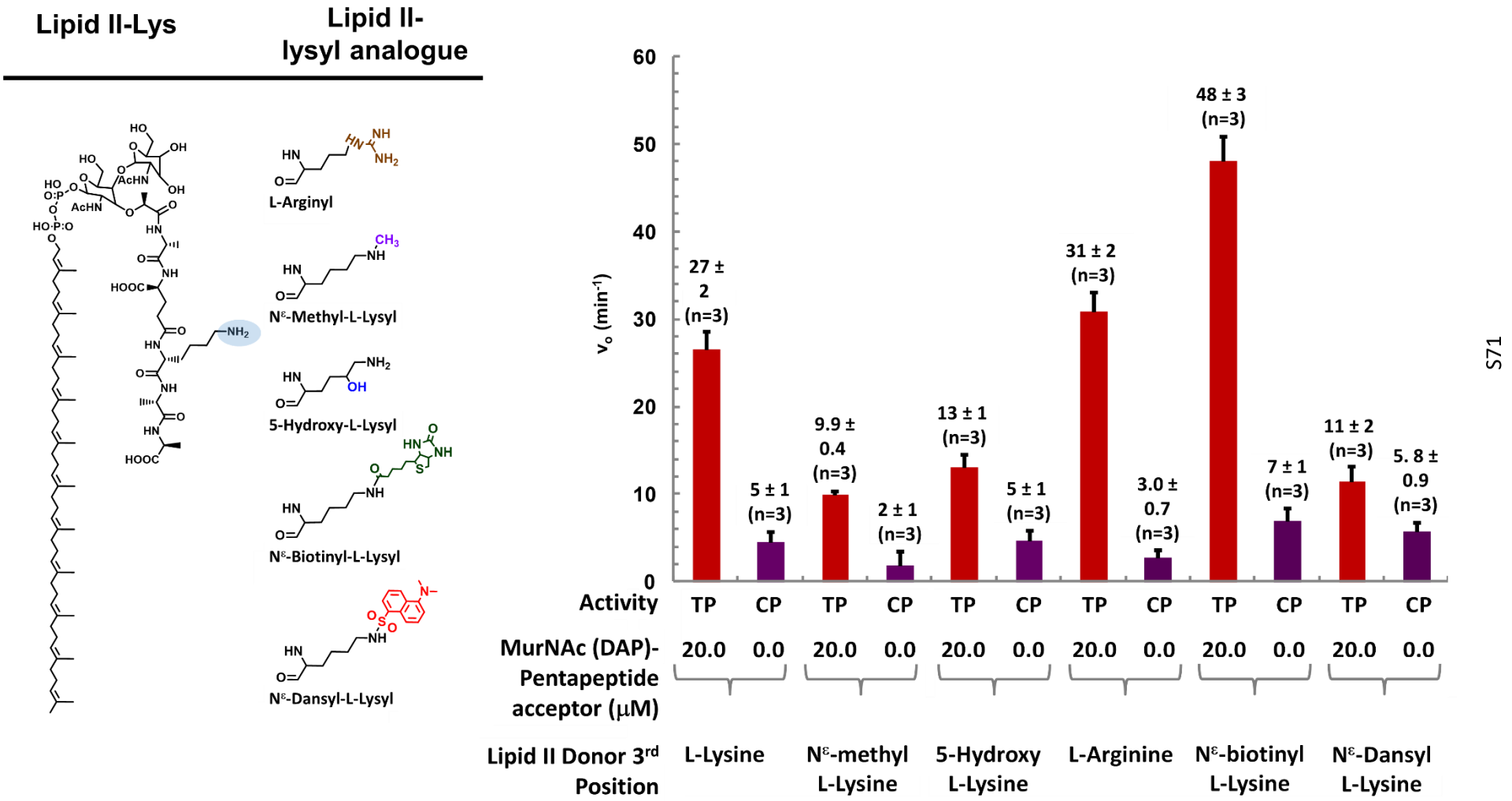

Figure S9

Impact of donor amidation on PBP1B activity

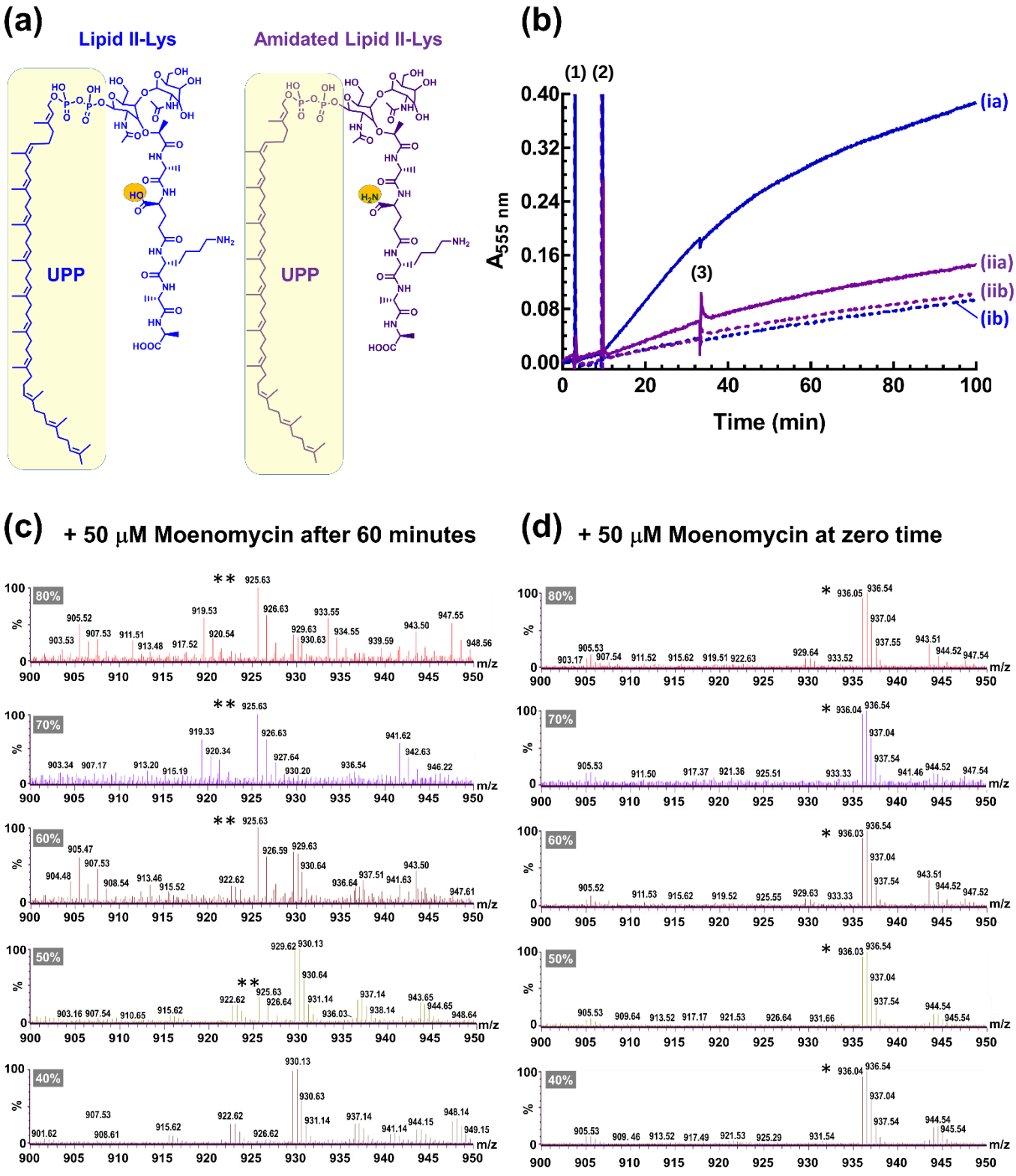

**: Undecaprenyl pyrophosphate expected (m-1)/1 = 925.62

*: Amidated lipid II-Lys expected (m-2)/2 = 936.03

Figure S10

Impact of substitution of *L*-alanine for *D*-alanine at the C-terminus of the stem peptide of the Lipid II-Lys transpeptidase donor of PBP1B

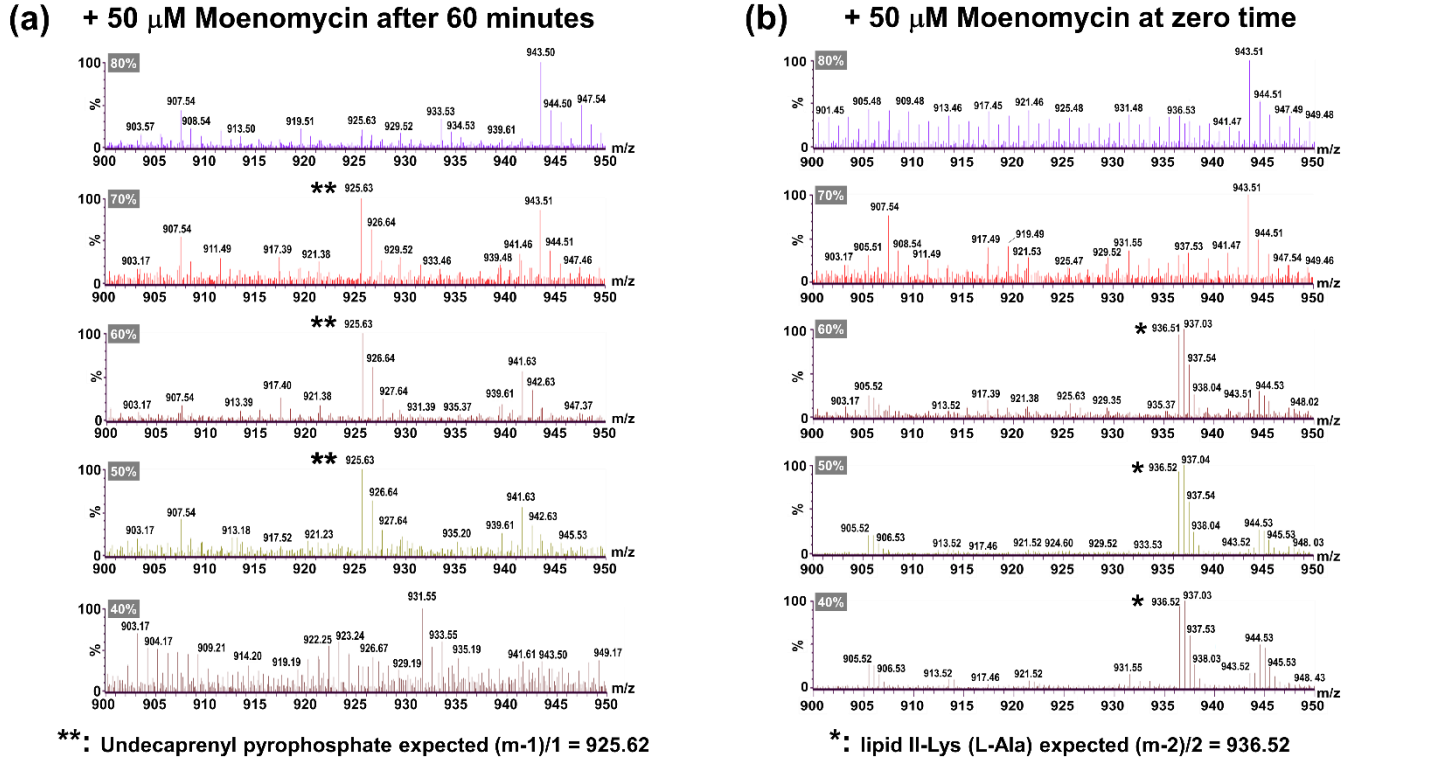

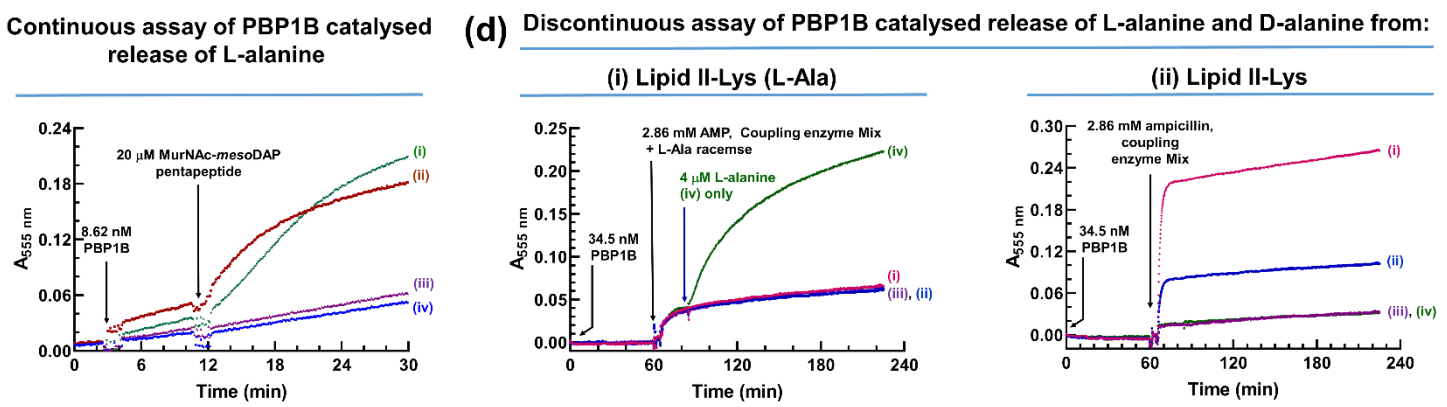

Figure S11

LCMSMS analysis of the structure of the transpeptidation products of PBP1B formed from lipid II-*L*,*L*-DAP and between lipid II-*L*,*L*-$^{\varepsilon}$NAc-DAP and MurNAc *meso*–DAP pentapeptide

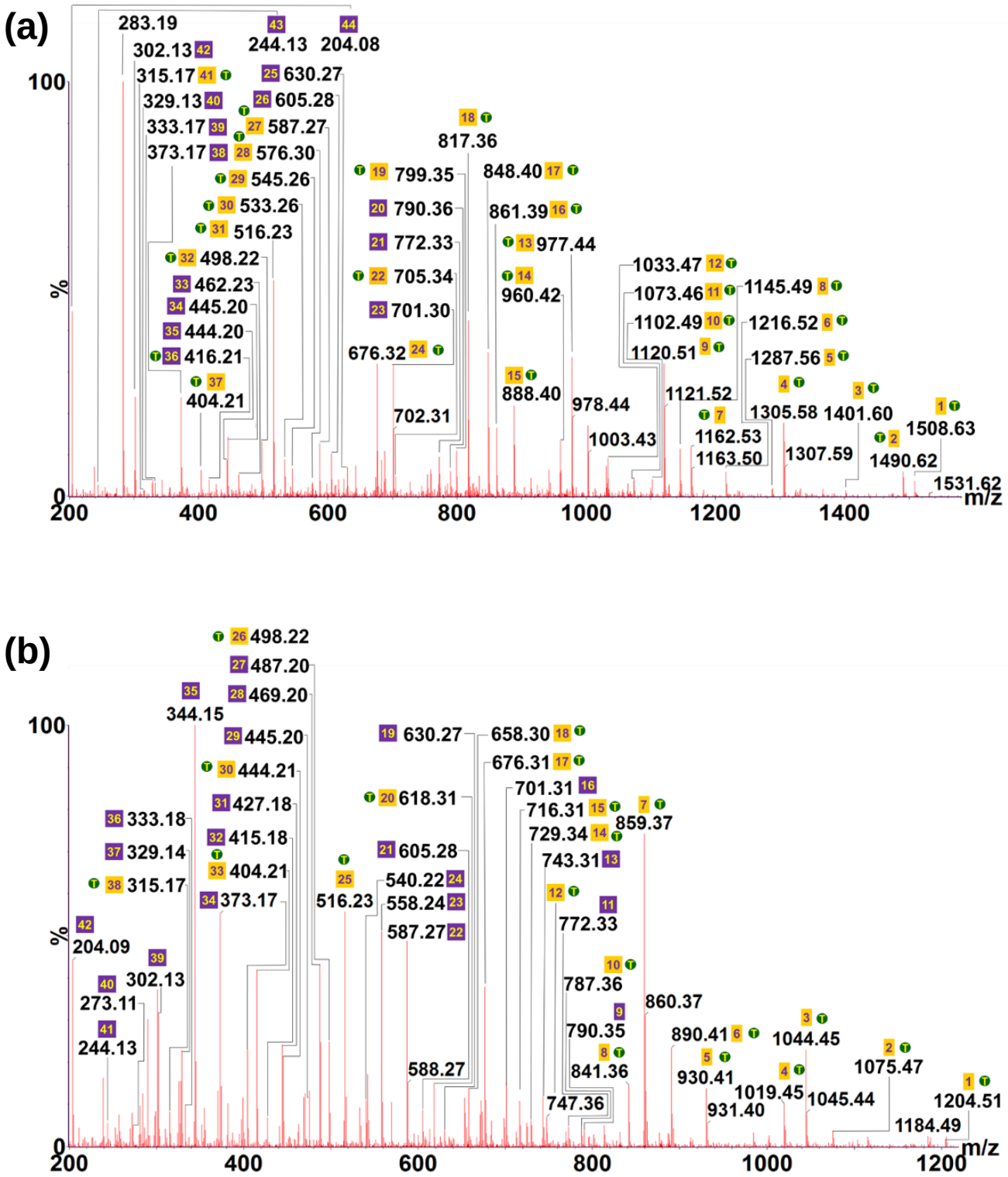

Figure S12

Variation of kinetics of acceptor utilization by PBP1B

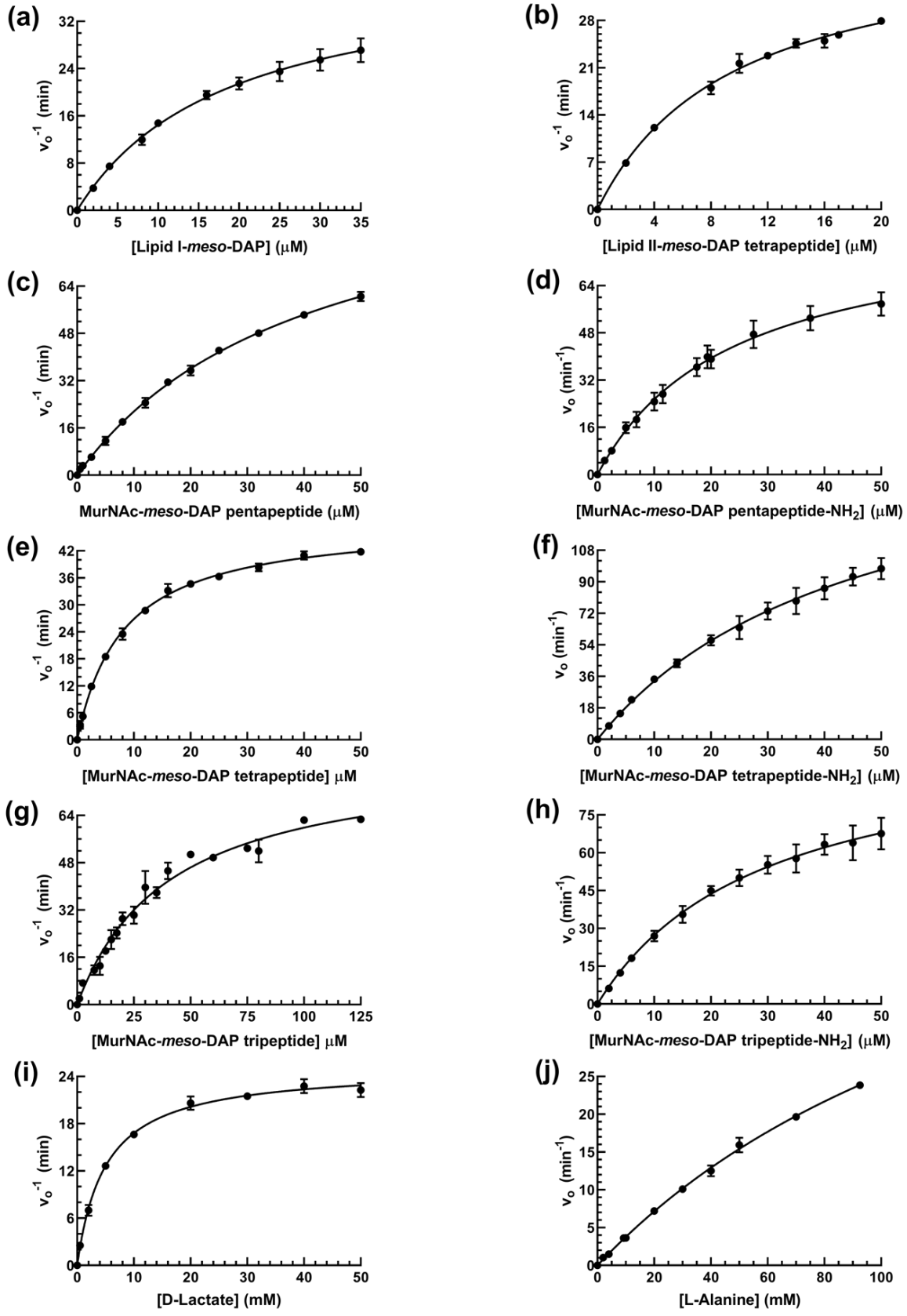

Figure S13

Theoretical relationships of v_o *vs* MurNAc *meso*-DAP tripeptide concentration at varying lipid II Lys described by equations 3 and S2-S4 fitted to experimental data

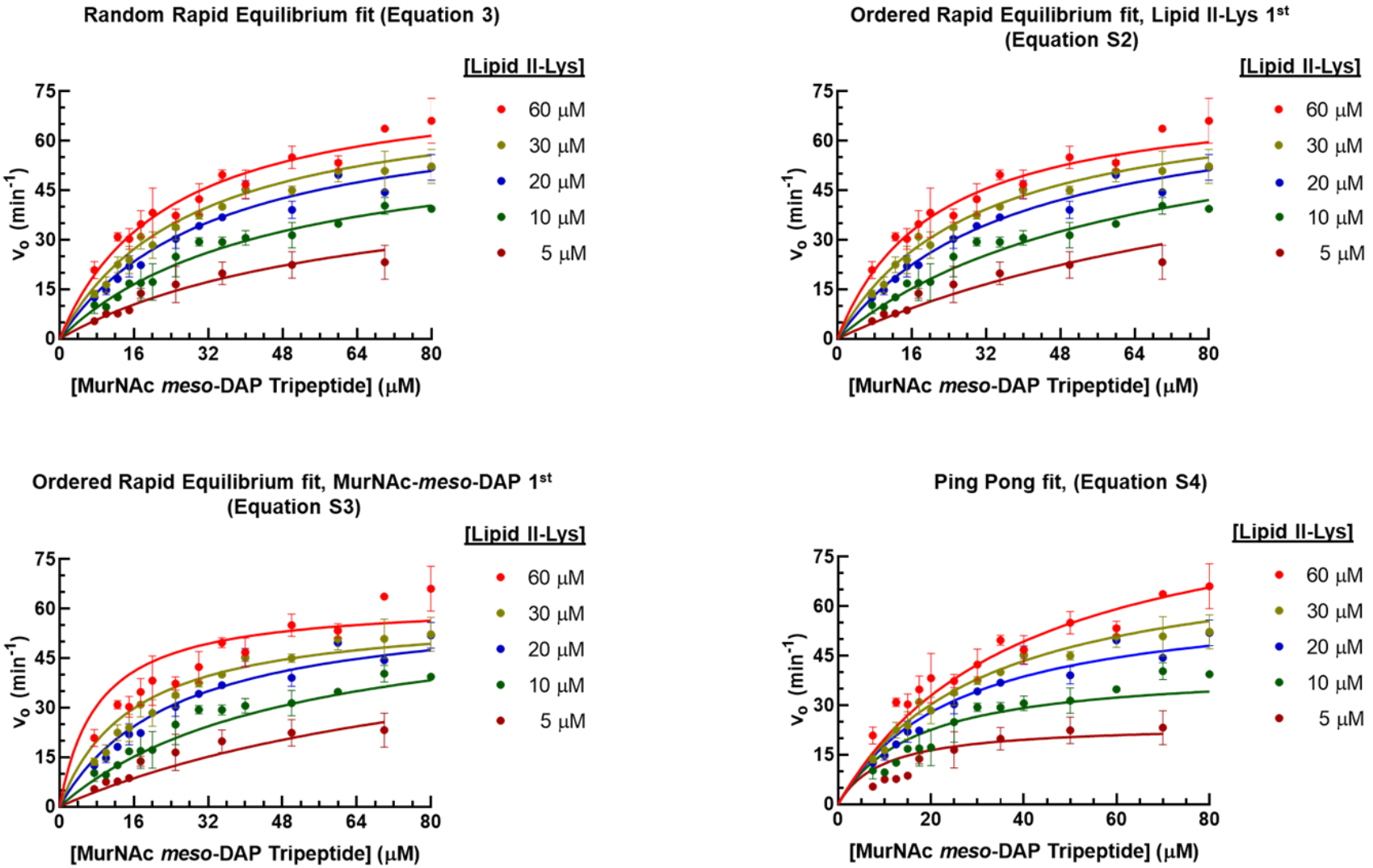

S.7: Supplementary References

S1. Bibi, S. Fabrication and use of D-serine biosensors for characterising D-serine signalling in rat brain. PhD Thesis, University of Warwick, United Kingdom, 2010.

S2. Miller, K.; Dunsmore C.J.; Leeds, J.A.; Patching, S,G.; Sachdeva, M.; Blake, K.L.; Stubbings, W.J.; Simmons, K.J.; Henderson, P.J.; De Los Angeles, J.; Fishwick, C.W.; Chopra, I. Benzothioxalone derivatives as novel inhibitors of UDP-N-acetyl-glucosamine enolpyruvyl transferases (MurA and MurZ). *J. Antimicrob. Chemother*. **2010**, 65 (12), 2566-2573.

S3. Crouvoisier, M.; Mengin-Lecreulx, D.; van Heijenoort, J. UDP-N-acetylglucosamine:N-acetylmuramoyl-(pentapeptide) pyrophosphoryl undecaprenol N-acetylglucosamine transferase from *Escherichia coli*: overproduction, solubilization, and purification. *FEBS Lett.* **1999,** 449 (2-3), 289-292.

S4. Huang, C.Y.; Shih, H.W.; Lin, L.Y.; Tien, Y.W.; Cheng, T.J.; Cheng, W.C.; Wong, C.H.; Ma, C. Crystal structure of *Staphylococcus aureus* transglycosylase in complex with a lipid II analog and elucidation of peptidoglycan synthesis mechanism. *Proc. Natl. Acad. Sci. USA* **2012,** 109 (17), 6496-6501.

S5. Punekar, A.S.; Samsudin, F.; Lloyd, A.J.; Dowson, C.G.; Scott, D.J.; Khalid, S.; Roper, D.I. The role of the jaw subdomain of peptidoglycan glycosyltransferases for lipid II polymerization. *Cell Surf.* **2018**, 2, 54-66.

S6. El Zoeiby, A.; Sanschagrin, F.; Havugimana, P.C.; Garnier, A.; Levesque, R.C. *In vitro* reconstruction of the biosynthetic pathway of peptidoglycan cytoplasmic precursor in *Pseudomonas aeruginosa*. *FEMS Microbiol*. *Lett*. **2001**, 201 (2), 229-235.

S7. Lloyd, A.J.; Gilbey, A.M.; Blewett, A.M.; De Pascale, G.; El Zoeiby, A.; Levesque, R.C.; Catherwood, A.C.; Tomasz, A.; Bugg, T.D.; Roper, D.I.; Dowson, C.G. Characterization of tRNA-dependent Peptide Bond Formation by MurM in the Synthesis of *Streptococcus pneumoniae* Peptidoglycan. *J. Biol. Chem.* **2008**, 283 (10), 6402-6417.

S8. Koo, C.W.; Blanchard, J.S. Chemical mechanism of *Haemophilus influenzae* diaminopimelate epimerase. *Biochemistry* **1999**, 38 (14), 4416-4422.

S9. Lloyd, A.J.; Brandish, P.E.; Gilbey, A.M.; Bugg, T.D. Phospho-N-acetyl-muramyl-pentapeptide translocase from *Escherichia coli*: catalytic role of conserved aspartic acid residues. *J. Bacteriol.* **2004**, 186 (6), 1747-1757.

S10. Terrak, M.; Ghosh, T.K.; van Heijenoort, J.; Van Beeumen, J.; Lampilas, M.; Aszodi J.; Ayala, J.A.; Ghuysen, J.M.; Nguyen-Distèche M. The catalytic, glycosyl transferase and acyl transferase modules of the cell wall peptidoglycan-polymerizing penicillin-binding protein 1b of *Escherichia coli*. *Mol. Microbiol*. **1999**, 34 (2), 350-364.

S11. Biboy, J.; Bui, N.K.; Vollmer, W. In Vitro peptidoglycan Synthesis Assay with Lipid II Substrate. *Meth. Mol. Biol.* **2013**, 966, 273-288.

S12. Dawson, R.M.C.; Elliot, D.C.; Elliot, W.H.; Jones, K.M. *Data For Biochemical Research*. 3rd Edition., Clarendon Press, Oxford, 1986.

S.13. Kishida, H.; Unzai, S.; Roper, D.I.; Lloyd, A.; Park, S.Y.; Tame, J.R. Crystal structure of penicillin binding protein 4 (*dacB*) from *Escherichia coli*, both in the native form and covalently linked to various antibiotics. *Biochemistry* **2006**, 45 (3), 783-792.

S.14 Agarwal**,** A.K. Design and synthesis of novel bacterial enzyme inhibitors as potential antituberculosis agents. PhD Thesis, University of Leeds, United Kingdom, 2007.

S15. Wijaya, E.C.; Separovic, F.; Drummond, C.J.; Greaves, T.L. Micelle formation of a non-ionic surfactant in non-aqueous molecular solvents and protic ionic liquids (PILs). *Phys. Chem. Chem. Phys.* **2016**, 18 (35), 24377-24386.

S16. Mesleh, M.F.; Rajaratnam. P.; Conrad, M.; Chandrasekaran, V.; Liu, C.M.; Pandya, B.A.; Hwang, Y.S.; Rye, P.T.; Muldoon, C.; Becker, B.; Zuegg, J.; Meutermans, W.; Moy, TI. Targeting Bacterial Cell Wall Peptidoglycan Synthesis by Inhibition of Glycosyltrans-ferase Activity. *Chem. Biol. Drug Des.* **2016**, 87 (2), 190-199.

S17. Brandish, P.E.; Burnham, M.K.; Lonsdale, J.T.; Southgate, R.; Inukai, M.; Bugg, T.D. Slow binding inhibition of phospho-N-acetylmuramyl-pentapeptide-translocase (*Escherichia coli*) by mureidomycin A. *J. Biol. Chem.* **1996**, 271 (13), 7609-7614.

S18. Shapiro, A.B.; Jahić, H.; Gao, N.; Hajec, L.; Rivin, O. A high-throughput, homogeneous, fluorescence resonance energy transfer-based assay for phospho-N-acetylmuramoyl-pentapeptide translocase (MraY). *J. Biomol. Screen.* **2012**, 17 (5), 662-672.

S19. Lloyd, A.J.. Citric Acid Cycle Enzymes of *Methylophilus methylotrophus.* PhD Thesis, University of Bath, United Kingdom, 1990.

S20. Breukink, E.; van Heusden, H.E.; Vollmerhaus, P.J.; Swiezewska, E.; Brunner, L.; Walker, S.; Heck, A.J.; de Kruijff, B. Lipid II is an intrinsic component of the pore induced by nisin in bacterial membranes. *J. Biol. Chem*. **2003**, 278 (22), 19898-19903.

S21. Clarke, T.B.; Kawai, F.; Park, S.Y.; Tame, J.R.; Dowson, C.G.; Roper, D.I. Mutational Analysis of the Substrate Specificity of *Escherichia coli* Penicillin Binding Protein 4. *Biochemistry* **2009**, 48 (12), 2675-2683.

S22. Zhou, M.; Diwu, Z.; Panchuk-Voloshina, N.; Haugland, R.P. A Stable Nonfluorescent Derivative of Resorufin for the Fluorometric Determination of Trace Hydrogen Peroxide: Applications in Detecting the Activity of Phagocyte NADPH Oxidase and Other Oxidases. *Analyt. Biochem.* **1997**, 253 (2)**,** 162–168.

S23. Helassa, N.; Vollmer, W.; Breukink, E.; Vernet, T.; Zapun, A. The Membrane Anchor of Penicillin-Binding Protein PBP2a From *Streptococcus pneumoniae* Influences Peptidoglycan Chain Length. **2012**, *FEBS J.* 279 (11), 2071– 2081.

S24. Barrett, D.; Wang, T.-S.A.; Yuan, Y.; Zhang, Y.; Kahne, D.; Walker, S. Analysis of Glycan Polymers Produced by Peptidoglycan Glycosyltransferases. **2007**, *J. Biol. Chem.* 282 (44), 31964–31971.

S25. Segel, I.H. Ch. 6. Rapid equilibrium bireactant and terreactant systems. B. Ordered bireactant systems in: *Enzyme Kinetics: Behavior and Analysis of Rapid Equilibrium and Steady-State Enzyme Systems;* Wiley Classics Library Edn. John Wiley & Sons, N. Jersey 1975, pp. 320-325.

S26. Segel, I.H. Ch. 6. Rapid equilibrium bireactant and terreactant systems. A. Random bireactant systems. A1 Initial velocity studies in: *Enzyme Kinetics: Behavior and Analysis*

of Rapid Equilibrium and Steady-State Enzyme Systems; Wiley Classics Library Edn. John Wiley & Sons, N. Jersey 1975, pp. 274-277.

S27. Walkowiak, G.P. The development of high-throughput assays and screening to enable the discovery of class A penicillin-binding proteins inhibitors. PhD Thesis, University of Warwick, August 2017.

S28. Copeland, R.A. Tight Binding Inhibitors. Ch. 9. in: *Enzymes: A Practical Introduction to Structure, Mechanism, and Data Analysis;* Wiley-VCH, New York 2000, pp. 310-313.